VOT 74271

DEVELOPMENT OF NONDESTRUCTIVE INSPECTION SYSTEMS USING INFRARED IMAGES BASED ON IMAGE PROCESSING TECHNIQUE

(PEMBANGUNAN SISTEM PEMERIKSAAN TANPAMUSNAH MENGGUNAKAN IMEJ INFRAMERAH BERDASARKAN TEKNIK PEMPROSESAN IMEJ)

SYED ABD. RAHMAN SYED ABU BAKAR

PUSAT PENGURUSAN PENYELIDIKAN
UNIVERSITI TEKNOLOGI MALAYSIA

2007

VOT 74271

DEVELOPMENT OF NONDESTRUCTIVE INSPECTION SYSTEMS USING INFRARED IMAGES BASED ON IMAGE PROCESSING TECHNIQUE

(PEMBANGUNAN SISTEM PEMERIKSAAN TANPAMUSNAH MENGGUNAKAN IMEJ INFRAMERAH BERDASARKAN TEKNIK PEMPROSESAN IMEJ)

SYED ABD. RAHMAN SYED ABU BAKAR

RESEARCH VOTE NO:
74271

Jabatan Mikroelektronik dan Kejuruteraan Komputer
Fakulti Kejuruteraan Elektrik
Universiti Teknologi Malaysia

2007

ACKNOWLEDGMENT

We would like to express our gratitude to Universiti Teknologi Malaysia for providing fruitful research environment and the government of Malaysia for supporting this research via MOSTI vote no. 74271, hence making this research run smoothly as expected.

Our appreciation also goes to MTBE Malaysia Sdn. Bhd., Gebeng, Kuantan, Malaysia for providing thermal images used in this project. Especially, to Faizal Abu Bakar for his care and helps in providing the required data.

DEVELOPMENT OF NONDESTRUCTIVE INSPECTION SYSTEMS USING INFRARED IMAGES BASED ON IMAGE PROCESSING TECHNIQUE

(*Keywords: Infrared thermography, thermal image, thresholding, defect detection*)

The last few years, infrared thermography technique has been applied successfully in petrochemical industry. The main information from this technology acquired by using infrared thermal camera is in the form of thermal image. Any abnormal condition of an inspected object will be reflected as an abnormal spot (often hotspot) at certain location in a thermal image with highest pixel intensity values. In image processing terminology, this spot is called as the defect. Current practice, this hotspot is interpreted manually by human inspector. This way of interpretation is not effective and efficient. This report proposes an automatic and efficient way for interpreting a thermal image, in term of defect detection. Local intensities operation (LIO) to highlight the defective area is applied before detecting defect by using a new thresholding scheme based on its minimum gray-level value in image histogram. From the experiments carried out, this technique can detect correctly any defect as depicted in a thermal image. After testing with twelve thermal images and comparing it with other defect detection algorithms, the proposed technique has the best performance with absolute error less than one percent (0.91%), while other algorithms produced an error as high as 66.80%. The proposed pre-processing local intensities operation also has made the standard defect detection algorithm, such as the Otsu technique, able to correctly detect the defect which may otherwise not be possible if it is done using non pre-processed (original) thermal image.

Key Researchers:

Assoc. Prof. Dr. Syed Abd. Rahman Syed Abu Bakar (Head)
Rudi Heriansyah

E-mail: syed@fke.utm.my
Tel. No.: 07-5535238
Vote No.: 74271

PEMBANGUNAN SISTEM PEMERIKSAAN TANPAMUSNAH MENGGUNAKAN IMEJ INFRAMERAH BERDASARKAN TEKNIK PEMPROSESAN IMEJ

(*Katakunci: Haba inframerah, imej haba, ambang, pengesanan kerosakan*)

Pada beberapa tahun terakhir, teknik haba inframerah telah berjaya diaplikasikan dalam industri petrokimia. Informasi utama dari teknologi ini yang diperoleh menerusi kamera haba inframerah adalah dalam bentuk imej haba. Sebarang keadaan tidak normal pada objek yang dikaji akan terserlah sebagai kawasan tak normal (seringkali kawasan panas) pada lokasi tertentu di imej haba dengan nilai piksel yang tinggi. Dalam terminologi pemprosesan imej, kawasan ini disebut sebagai kerosakan. Pada masa sekarang ini, kawasan panas ini diterjemahkan oleh manusia. Cara penterjemahan sebegini tidak efisien dan efektif. Lapuran ini mencadangkan satu cara automatik dan efisien untuk mengterjemahkan kerosakan yang ada pada imej haba berkenaan. Operasi intensiti tempatan yang diterapkan sebelum pengesanan kerosakan menggunakan satu proses ambang baru berdasarkan nilai minima tingkat keabuan pada histogram imej. Ujikaji yang telah dilakukan menunjukkan bahawa teknik ini dapat mengesan secara automatik dan efisien sebarang kerosakan yang ada. Setelah percubaan dilaksanakan menggunakan dua belas imej haba dan dibandingkan dengan teknik pengesan kerosakan yang lain, teknik yang dicadangkan menunjukkan prestasi yang terbaik dengan perbandingan mutlak ralat kurang dari satu peratus (0.91%), berbanding dengan algoritma lain yang memberikan ralat sebesar 66.80%. Operasi intensiti tempatan yang dicadangkan juga dapat menjadikan algoritma piawai seperti teknik Otsu, mampu mengesan kerosakan dengan betul yang sebelumnya tidak mungkin dilakukan jika menggunakan tanpa pra-pemprosesan atau imej haba asal.

Penyelidik:

Assoc. Prof. Dr. Syed Abd. Rahman Syed Abu Bakar (Ketua)
Rudi Heriansyah

E-mail: syed@fke.utm.my
Tel. No.: 07-5535238
Vote No.: 74271

TABLE OF CONTENTS

GLOSSARY OF TABLES

GLOSSARY OF FIGURES

LIST OF ABBREVIATIONS

1-D	–	1 Dimension
2-D	–	2 Dimension
ACO	–	Ant Colony Optimization
FCM	–	Fuzzy C-Means
IRT	–	Infrared Thermography
LIL	–	Local Intensities Lighting
LIO	–	Local Intensities Operation
LIW	–	Local Intensities Weighting
LW	–	Long Wave
MAT	–	Midway Absolute Thresholding
MFT	–	Minimum Frequency Thresholding
MRT	–	Midway Relative Thresholding
NDE	–	Nondestructive Evaluation
PdM	–	Predictive Maintenance
PM	–	Preventive Maintenance
PSO	–	Particle Swarm Optimization
SW	–	Short Wave

LIST OF PUBLICATIONS

JOURNAL

- Rudi Heriansyah, U. U. Sheikh, and S. A. R. Abu-Bakar. (2007). 2-D Automatic Composition of Nodal Values in a Numerical Model Using Spreadsheet Programming. *Jurnal Teknologi.* C. (On review)

- Rudi Heriansyah, U. U. Sheikh, and S. A. R. Abu-Bakar. (2007). Synthetic Thermal Image Generation using Numerical Heat Transfer Modeling. *Jurnal Teknologi.* D. (On review)

- Rudi Heriansyah and S. A. R. Abu-Bakar. (2007). Defect Detection in Thermal Image using Local Intensities Operation and Minimum Frequency Thresholding. *Pattern Recognition Letters.* Elsevier, Ltd. (In preparation for submission)

CONFERENCE PROCEEDINGS

- Rudi Heriansyah and S. A. R. Abu-Bakar. (2007). Modeling of Defects within High Temperature Wall by Means of Infrared Thermography. *Proceedings of International Conference on Risk Technology 2007 (RISKTech '07).* Bandung, Indonesia: Mar. 24-27, 2007. 298-302.

- Rudi Heriansyah and S. A. R. Abu-Bakar. (2007). Defect Depth Estimation in Passive Thermography: Comparing Multilayer Perceptrons with Radial Basis Functions Networks. *Proceedings of Malaysia Japan International Symposium on Advance Technology 2007* (*MJISAT 2007*). Kuala Lumpur, Malaysia: Nov. 12-15, 2007. (Invited paper, accepted for publication)

- Rudi Heriansyah and S. A. R. Abu-Bakar. (2007). Defect Depth Estimation in Passive Thermography using Neural Network Paradigm. *Proceedings of the*

WSEAS 6th International Conference on Circuits, Systems, Electronics, Controls & Signal Processing 2007 (*CSECS '07*). Cairo, Egypt: Dec. 29-31, 2007. (Paper ID: 568-735, accepted for publication)

- Rudi Heriansyah and S. A. R. Abu-Bakar. (2007). Defect Detection in Thermal Image using Thresholding Technique. *Proceedings of the WSEAS 6th International Conference on Circuits, Systems, Electronics, Controls & Signal Processing 2007* (*CSECS '07*). Cairo, Egypt: Dec. 29-31, 2007. (Paper ID: 568-736, accepted for publication)

CHAPTER 1

INTRODUCTION

1.1 Background

Infrared thermography (IRT) (Kaplan, 1993), (Maldague, 1993), (Gaussorgues, 1994), (Maldague, 2001) is one of many existing nondestructive testing techniques for preventive (PM) or predictive maintenance (PdM) (Mobley, 1990), (Gardner, 1992), (Levitt, 2003).

In the last few decades, IRT has gained much attention and has been successfully applied to the areas of electrical, mechanical, petrochemical, building and structures, material testing, industry, medical, and many others various applications (Kaplan, 1993) ranging from breast cancer detection (Qi *et al.*, 2002) to SARS (severe acute respiratory syndrome) diagnosis (Wang *et al.*, 2004), from aircraft inspection (D'Orazio *et al.*, 2005) to buildings application (Lo and Choi, 2004). Among others, the popularity of IRT lies in its contactless, easy to interpret the thermal data, large area of inspection, free from dangerous radiation.

One area where IRT has played an important role is in the petrochemical industry. This type of industry is categorized as a heavyweight industry with high investment cost, operational cost, and maintenance cost, along with high requirement for safety. Any problem found in running facilities should be known earlier since breakdown of equipment will affect other equipments or even the entire operation of the plant. Maintenance should be scheduled properly and regularly because shutdown or startup equipment cannot be done suddenly as it is related to operational cost. Petrochemical site is a hazardous area, therefore entering this site should adhere to the safety standard. Because of these conditions the PdM and nondestructive evaluation (NDE) technique using IRT with its remote access capability have more advantageous over other PdM schemes.

Several big petrochemical industry players such as BP Amoco (Nyholt, 2000), Texaco (Ohliger and Alvarado, 2001) and Chevron Texaco (Ohliger, 2002) have taken the benefit of IRT technology. One example of local petrochemical company that uses this technology in its predictive maintenance program is MTBE Malaysia Sdn. Bhd., located at Gebeng, Kuantan, Pahang, Malaysia. All thermal images used in this report have been provided by this company.

Other applications of IRT in petrochemical industries, refineries, or facilities, are in the inspection of tanks (Sims, 2001), boilers (May, 2003), process vessels (Bonin, 2003), horsehead (beam) pump (Ohliger, 2003), lagged pipe (Willis, 2004), furnace tube (LeClercq, 2003), refractory lined petroleum refinery equipment (Whitcher, 2004), and process heaters (Weigle, 2005). These various applications show that IRT is a suitable tool for petrochemical industry applications.

1.2 Motivation

Thermal data is the main source when employing IRT technology. This data can be in the form of a single numerical value when using point sensing infrared equipment or many numerical values (or pixel values) when using area sensing equipment (Kaplan, 1993). This numerical value represents the temperature quantity. For visualization purpose, these temperature values are converted into pixel values in the form of thermal image. Any abnormal condition on the inspected object will be reflected by unusual temperature distribution. This abnormal temperature pattern will be depicted as either a cluster of bright pixels or dark pixels. This brightest spot in visual inspection terminology is referred to as *defect*. In this report, the brightest defect spot is referred to as a *hot* defect, and the darkest defect spot is referred to as a *cold* defect. Chapter 2 will discuss further details on these defects.

In current practice, the interpretation of the thermal image in many applications are done manually using human interpretation. Some efforts have been made to automate the interpretation for this thermal data (Maldague, 2001). However, up to the point of writing this report, there has been no automated interpretation in the petrochemical application. Most of the data are analyzed

qualitatively using human vision system. This report thus proposes an automatic way for interpreting thermal image in term of defect detection.

1.3 Objective

The objective of this work is to develop an algorithm that can automatically detect defects as depicted in thermal images and implement this algorithm in a programming language. Image processing paradigm is the main tool for algorithm development. For verification purpose, the developed algorithm and its implementation are tested with thermal image dataset both for the case of *hot* and *cold* defects. A benchmarking procedure is also designed for performance evaluation of the developed algorithm along with comparison with existing techniques.

1.4 Scope of Work

This work is limited to the following scopes:

- Thermal data used is in the form of pixel values of thermal image.
- Thermal image is obtained from passive thermography scheme meaning that no time dependency from one thermal image to another, hence no thermal contrast computation is needed.
- Thermal image is in 8-bits format (256 gray-level value).

1.5 Contributions

The first contribution of this report is in the development of pre-processing algorithm for defect visibility enhancement and gray-level value localization in image histogram. Local intensities operation (LIO) using 3×3 window neighborhood pixel value is proposed. LIO operation comes in two schemes: local intensities weighting (LIW) operation for use in detection hot defect and local intensities lighting (LIL) operation for use in detection of cool defect.

The second contribution is the development of the thresholding algorithm based on 1-D image histogram. Rather than using the 2-D histogram, 1-D histogram

is selected due to its simplicity and fast processing computation. Three simple thresholding algorithms based on midway absolute thresholding (MAT), midway relative thresholding (MRT), and minimum frequency thresholding (MFT) are proposed to detect defect in thermal image after LIO pre-processing operation. LIO operation combined with these proposed algorithms are found to outperform other techniques (this result is given in Chapter 4).

The third contribution is in tailoring LIO pre-processing operation with any non-dedicated thermal image defect detection algorithm. This combination has enables the defects to detected which were otherwise not possible without the combination with LIO.

1.6 Report Organization

The report is organized as follows. Chapter 2 provides a short description on terminology which is commonly used in infrared thermography and thermal image data. This chapter also provides review on existing non-dedicated and dedicated algorithms based on thresholding technique which are commonly used for background and foreground separation or object detection. Chapter 3 discusses the proposed algorithms for thermal image pre-processing and thresholding algorithm for defect detection. Experimental results to verify the proposed algorithms are given in Chapter 4. This chapter also gives the benchmarking result of the proposed defect detection algorithms against other existing algorithms. The last Chapter 5 summarizes and concludes the report and gives recommendation for future work.

CHAPTER 2

LITERATURE REVIEW

2.1 Overview

This chapter reviews some of the existing techniques devoted to detect defects as depicted in a thermal image. The advantages and disadvantages of each technique are highlighted. A brief discussion on materials related with thermal image is also given in the text.

2.2 Thermal Image

The *infrared thermal image* or in shortl *thermal image* is an image which is captured using an *infrared thermal camera* or simply *thermal camera* (not to confuse with an *infrared camera* which is commonly applied for a night vision application). Essentially this device captures electromagnetic spectrum within infrared bands (0.78 – 1000 μm) (Figure 2.1). Therefore, unlike the intensity image which is lies within the visible light, a thermal image is a function of radiated energy of an inspected object (Kaplan, 1993). This is illustrated in Figure 2.2.

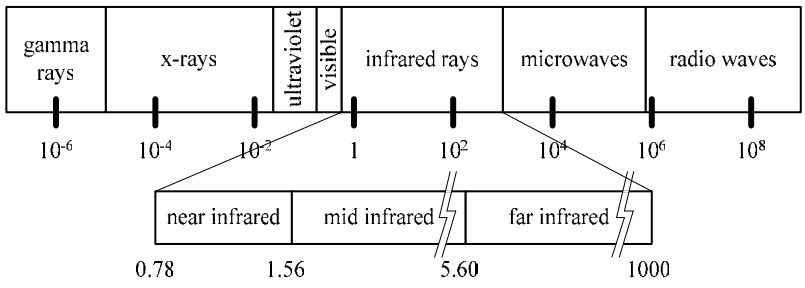

Figure 2.1 Electromagnetic spectrum

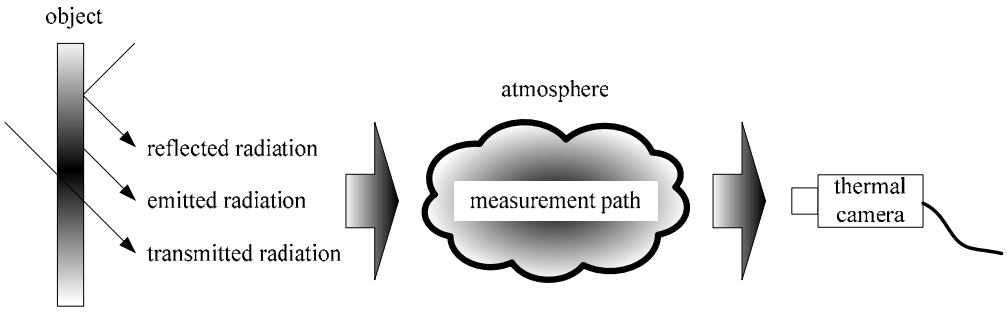

Figure 2.2 Thermal image as a function of energy radiation

According to its working wavelength, thermal camera can be divided into two groups: *short wave* and *long wave* thermal cameras. A short wave (SW) camera operates in bands between 3 and 5 μm and a long wave (LW) camera operates in bands between 8 and 12 μm. The LW camera is of particular interest for measuring radiation from objects at room temperature (an example is for the detection of intruders by law enforcement agencies). The SW camera is best suited for warmer objects (an example is any process releasing CO_2, such as combustion engines) (Maldague, 2001).

Raw data captured by a thermal camera is in the form of temperature values. Thermal camera manufacturer usually has their own software to read this data and display them as a thermal image. When converting temperature values into thermal image, a pseudo-coloring or false-coloring technique (Chanda and Majumder, 2000) is used.

Certain color level represents certain temperature values. In this software terminology, this color map is called *palette*. IRBIS and IRBIS Plus V2.2 (from InfraTec GmbH Dresden) has seven palettes: *varioscan*, *varioscan printer*, *black → white*, *white → black*, *iron*, *blue → red*, and *stufen*. While ThermaCAM Explorer 99 (from FLIR Systems) offers more various palettes: *glowbow*, *grey*, *grey10*, *greyred*, *iron*, *iron10*, *medical*, *midgreen*, *midgrey*, *rain*, *rain100*, *rain900*, and *yellow*. Figure 2.3 shows a visible image along with its thermal image in several palettes from ThermaCAM Explorer 99.

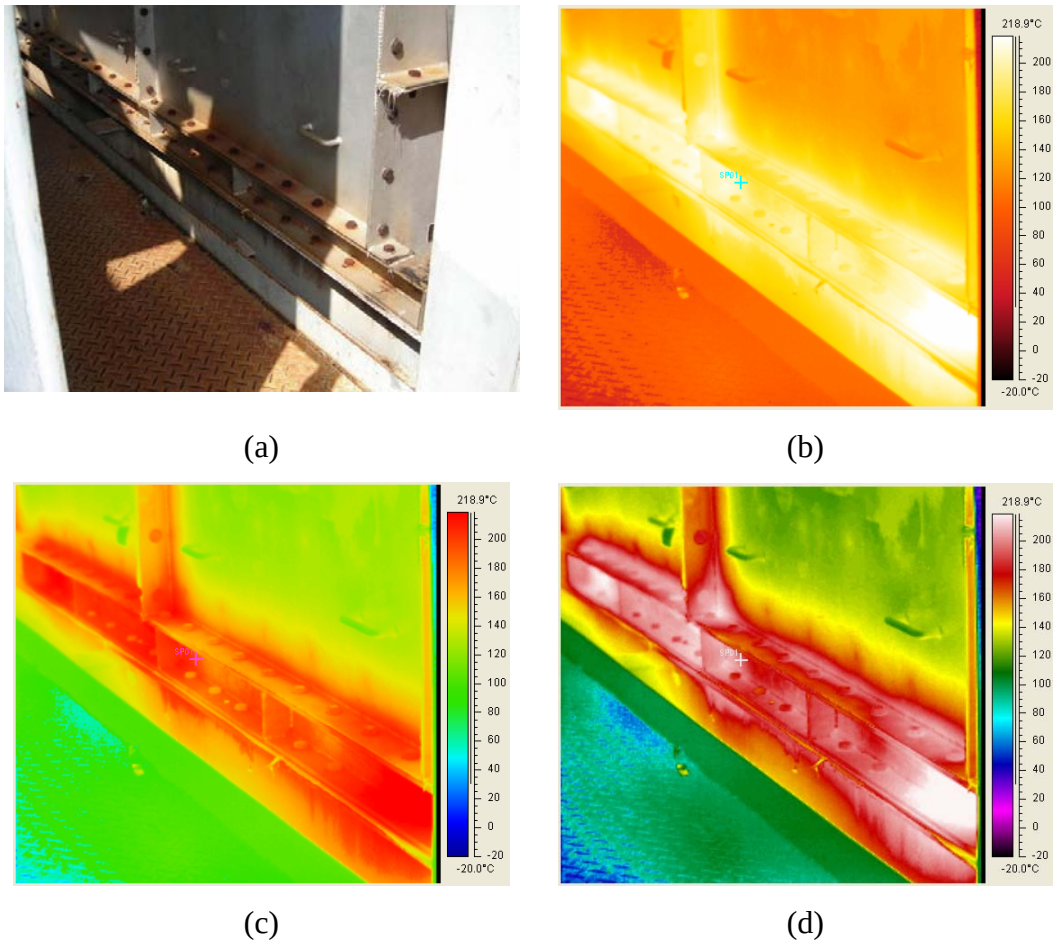

Figure 2.3 (a) Visible image with its thermal image (b) *glowbow*, (c) *midgreen* and (d) *rain* palette

2.3 Defect in Thermal Image

In a thermal image, a defective area or an area with the hottest temperature is usually represented by the brightest color. Sometimes, the defective area is represented by the darkest color. In this report, the hot defective area is called as *hot defect*, and the cold defective area is called as *cold defect*.

To save the computational cost, rather than working in a colored thermal image, this report takes the advantage of using a grayscale thermal image, since the defective area is still obvious in this mode. Figure 2.4 shows a color thermal image and grayscale thermal image, the defective area (as depicted with bright color in this

image) is still clearly differentiable with the background for both images as shown by the intensities profile over the defective area.

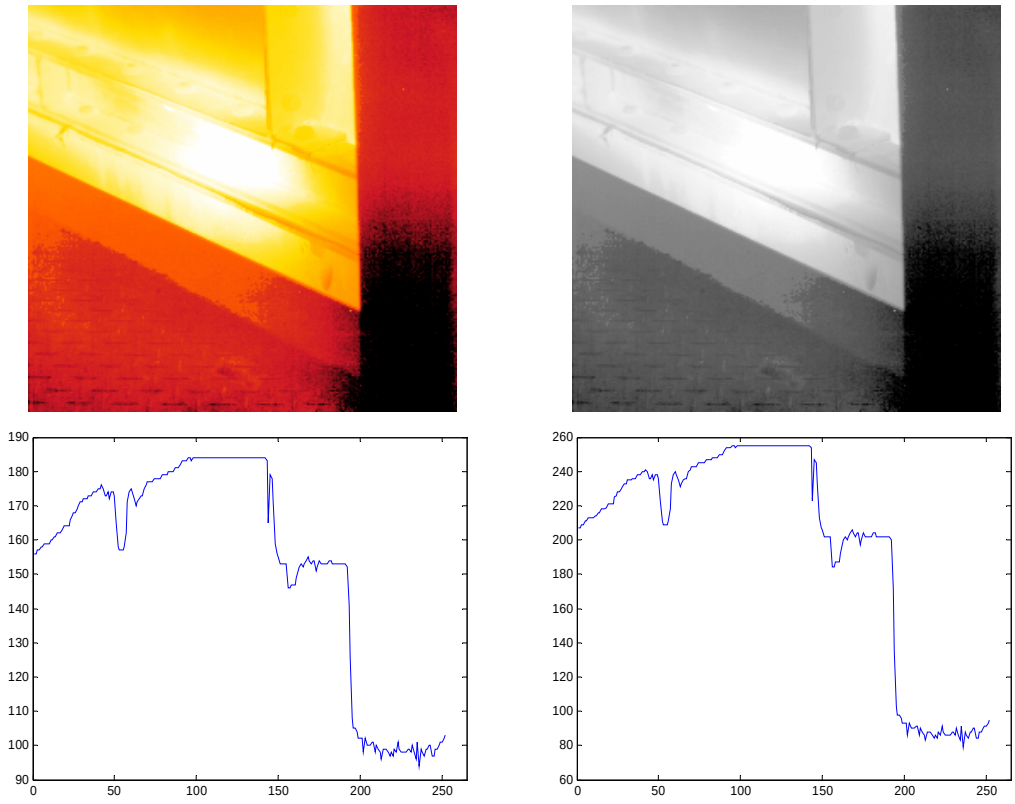

(a) (b)

Figure 2.4 (a) Color thermal image, (b) grayscale thermal image with their intensity profile over the defect area

2.4 Thresholding Algorithms

Image thresholding is mostly used for image segmentation due to its intuitive properties and easy to implement (Gonzalez and Woods, 2002). Thresholding also is a common tool for defect detection (Ng, 2006).

Thresholding is a process to separate object from its background in a digital image. Histogram is the main tool in this separation process. Suppose that the gray-level histogram shown in Figure 2.5 corresponds to an image, *f(x,y)*, composed of light objects on a dark background, in such a way that object and background pixels

have gray levels grouped into two dominant modes. One obvious way to extract the objects from the background is to select a threshold *T* that separates these modes. A thresholded image *g*(*x*,*y*) from an image *f*(*x*,*y*) is defined as:

$$g(x,y) = \begin{cases} 1 & \text{if } f(x,y) > T \\ 0 & \text{if } f(x,y) \le T \end{cases} \tag{2.1}$$

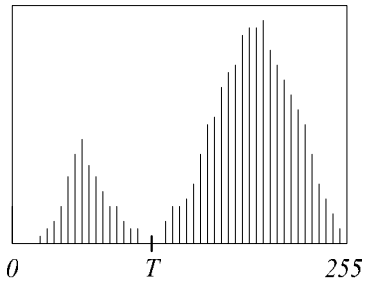

Figure 2.5 Gray-level histogram to separate object from its background

If the gray-level histogram is calculated from the entire image, then value *T* is called a *global* threshold. Otherwise, if the histogram derived from a local window pixel values then it is called a *local* threshold. If only one *T* value is needed then it is called *bi-level* thresholding, if more than one *T* values are needed than it is called *multi-level* thresholding (Chanda and Majumder, 2000), (Ritter and Wilson, 2001), (Gonzalez and Woods, 2002).

Numerous thresholding techniques for image segmentation have been proposed and the surveys of these techniques have been published elsewhere (Weszka and Rosenfeld, 1978), (Sahoo *et al.*, 1988), (Lee *et al.*, 1990), (Glasbey, 1993), (Sezgin and Sankur, 2004). Some criteria for performance evaluation of these thresholding techniques were also described in these papers.

Sezgin and Sankur (2004) have classified these thresholding techniques into six categories: (1) histogram shape-based methods, (2) clustering-based methods, (3) entropy-based methods, (4) object attributed-based methods, (5) the spatial methods, and (6) local methods.

Otsu (1979) proposed a thresholding technique which is commonly also recognized as *maximum between-class variance* (BCV) method (clustering-based category). It is one of the popular global thresholding method due to its simplicity (Lin, 2002), (Du *et al.*, 2004). Otsu method was successfully applied to text document (Wu and Amin, 2003) in which the background and foreground for this image is bi-modal in nature, but this method could fail for an extremely unbalanced sizes of background-foreground classes as shown by Kittler and Illingworth (1985). Otsu method also is a global thresholding method. This method will face a problem if the image has uneven illumination.

In Otsu method, an image with gray level histogram $\{p_i\}_{i=0}^{L}$ is thresholded at *T* gray level value. The probabilities of background and foreground of the *T*-thresholded image can be calculated:

$$P_B(T)=\sum_{i=0}^{T} p_i \quad \text{and} \quad P_F(T)=1-P_B(T)=\sum_{i=T+1}^{L-1} p_i \tag{2.2}$$

From Equation (2.3), the means and variances associated with the background and the foreground can be further calculated by:

$$\mu_B(T)=\frac{\sum_{i=0}^{T} i\times p_i}{P_B(T)} \quad \text{and} \quad \mu_F(T)=\frac{\sum_{i=T+1}^{L-1} i\times p_i}{P_F(T)} \tag{2.3}$$

$$\nu_B(T)=\frac{\sum_{i=0}^{T} (i-\mu_B(T))^2\times p_i}{P_B(T)} \quad \text{and} \quad \nu_F(T)=\frac{\sum_{i=T+1}^{L-1} (i-\mu_F^T)^2\times p_i}{P_F(T)} \tag{2.4}$$

Between-class and *within-class variance*, can then be defined as:

$$\nu_{between-class}(T)=P_B(T)\times P_F(T)\times(\mu_B(T)-\mu_F(T))^2 \tag{2.5}$$

$$\nu_{within-class}(T)=P_B(T)\times\nu_B(T)+P_F(T)\times\nu_F(T) \tag{2.6}$$

Optimum thresholding value in Otsu's method is determined by maximizing $\nu_{between-class}^{T}$ or minimizing $\nu_{within-class}^{T}$ as in the following equation:

$$T = \arg\left\{\max_{1\le T\le L}\left(\nu_{between-class}(T)\right)\right\} \quad \text{or} \quad T = \arg\left\{\min_{1\le T\le L}\left(\nu_{within-class}(T)\right)\right\} \quad (2.7)$$

Ridler and Calvard (1979) proposed a cluster-based thresholding algorithm without using image histogram. An initial guess at a threshold is refined consecutive passes through the image.

The initial guess at the threshold is simply the mean gray level. This threshold is then used to collect statistics on the black and white regions obtained; the mean gray-level for all pixels below the threshold is found an called T_b, and the mean level of the pixels greater than or equal to the initial threshold is called T_o. Now a new estimate of the threshold is computed as $(T_b + T_o)/2$, or the average of the mean levels in each pixel class, and the process is repeated using this threshold. When no change in threshold is found in two consecutive passes through the image, the process stops.

Kapur *et al.* (1985) proposed a gray-level thresholding using the entropy of the histogram. Entropy is the measure of information content. In this technique, the image foreground and background are considered as two different signal sources, so that when the sum of the two class entropies reaches its maximum, the image is said to be optimally thresholded.

$$T = \arg\left\{\max_{1\le T\le L}\left(H_B(T) + H_F(T)\right)\right\} \quad (2.8)$$

where

$$H_B(T) = -\sum_{i=0}^{T}\frac{h(i)}{P(T)}\log\frac{h(i)}{P(T)} \quad (2.9a)$$

$$H_F(T) = -\sum_{i=T+1}^{255}\frac{h(i)}{P(T)}\log\frac{h(i)}{P(T)} \quad (2.9b)$$

Tsai (1985) used moment-preserving principle for determining optimal threshold value. In this technique, the gray-level image is considered as the blurred version of an ideal binary image. The thresholding is established so that the first

three gray-level moments match the first three moments of the binary image. The gray-level moments m_k and binary image moments b_k are defined as:

$$m_k = \sum_{g=0}^{G} p(g) g^k \quad \text{and} \quad b_k = P_f m_f^k + P_b m_b^k \tag{2.10}$$

Kittler and Illingworth (1986) created a criterion function in which the minimum of this function is the best threshold:

$$T = J_B - J_T \tag{2.11}$$

where

$$J_B = 1 + 2\left(P_B(T) \log \sigma_B(T) + P_F(T) \log \sigma_F(T)\right) \tag{2.12}$$

$$J_F = 1 + 2\left(P_B(T) \log P_B(T) + P_F(T) \log P_F(T)\right) \tag{2.13}$$

and

$$P_B(T) = \sum_{i=0}^{T} h(i) \tag{2.14a}$$

$$P_F(T) = \sum_{i=T+1}^{255} h(i) \tag{2.14b}$$

$$\sigma_B^2(T) = \frac{\sum_{i=0}^{T} h(i)\left(i - \mu_B(T)\right)^2}{P_B(T)} \tag{2.15a}$$

$$\sigma_F^2(T) = \frac{\sum_{i=T+1}^{255} h(i)\left(i - \mu_F(T)\right)^2}{P_F(T)} \tag{2.15b}$$

with

$$\mu_B(T) = \frac{\sum_{i=0}^{T} i \times h(i)}{P_B(T)} \tag{2.16a}$$

$$\mu_F(T) = \frac{\sum_{i=T+1}^{255} i \times h(i)}{P_F(T)} \tag{2.16b}$$

This technique in the literature is usually referred to as a *minimum error thresholding* (MET) technique. According to the study conducted by Sezgin and Sankur (2004), MET is the best performing algorithm competed to other 40 thresholding techniques, both for nondestructive testing (NDT) images and document images.

Abutaleb (1989) with its 2-D histogram based takes account the spatial correlation between pixels in the image for thresholding determination. This work was an extension from the 1-D entropy method to its 2-D version. If g is the gray-level value of a pixel and $\bar{g}$ is the average gray level value of a neighborhood centered at that pixel, by using the 2-D histogram $p(g, \bar{g})$, for any threshold pair $(T, \bar{T})$, the cumulative distribution $P(T, \bar{T})$ can be calculated and defined the foreground entropy as:

$$Hf = -\sum_{i=1}^{T}\sum_{j=1}^{\bar{T}} \frac{p(g,\bar{g})}{P(T,\bar{T})} \log \frac{p(g,\bar{g})}{P(T,\bar{T})} \text{a} \tag{2.17}$$

By the same way, the second order entropy of background region can be derived. Under the assumption that the off-diagonal terms, that is the two quadrants $[(0,T),(\bar{T},G)]$ and $[(T,G),(0,\bar{T})]$ are negligible and contain elements only due to image edges and noise, the optimal pair $(T, \bar{T})$ can be found as the minimizing value of the 2-D entropy function.

Recently, Ng (2006) proposed a modified version of Otsu method. This algorithm was designed to detect small defective pattern on an image. The alternative formulation of Otsu method as defined by Liao *et al.* (2001) is:

$$T = \arg\left\{\max_{1 \le T \le L}\left(P_B(T) \times \mu_B^2(T) + P_F(T) \times \mu_F^2(T)\right)\right\} \tag{2.18}$$

The modified criterion function is then:

$$T = \arg\left\{\max_{1\le T\le L}\left(1-p_t\right)\left(P_B(T)\times\mu_B^2(T)+P_F(T)\times\mu_F^2(T)\right)\right\} \qquad (2.19)$$

where p_t is the probability of occurrence at the threshold value and it should be the small value to detect small defect.

The methods described here are global thresholding techniques. They are generally designed for segmentation of visible images. The method proposed by Ng (2006) was designed to work on detecting small defect on an image for the application of visual inspection.

Figure 2.6 clearly shows that the traditional thresholding techniques may not feasible for thermal images, since the nature of a thermal image is quite different from that of a conventional intensity image (Chang *et al.*, 1997), especially for specific application likes defect detection.

This figure also shows that Otsu and Ridler methods have quite similar result. Kapur method (in this example) give a false-positive thresholding. Tsai and Ng method seems to give quite similar results.

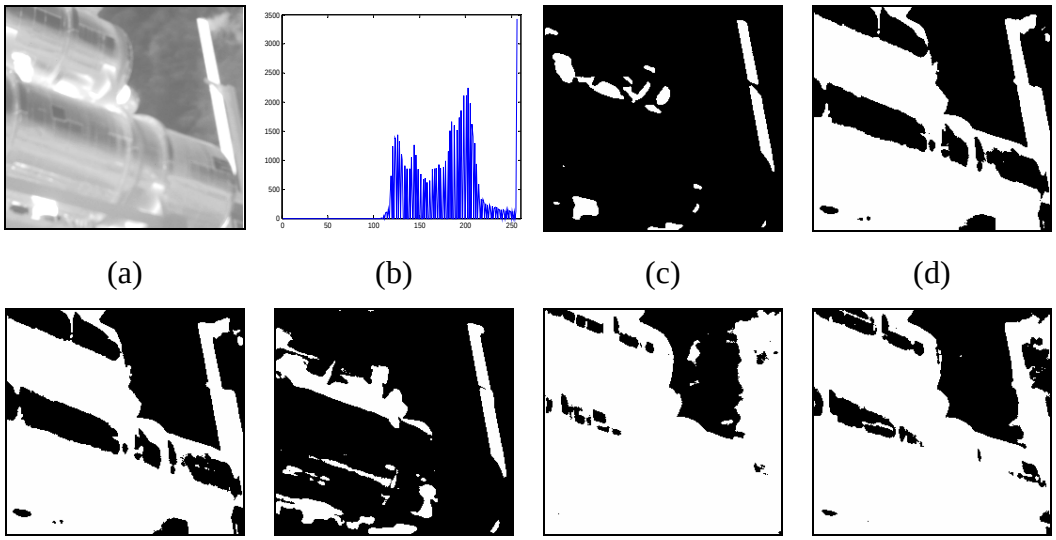

Figure 2.6 (a) Thermal image, (b) histogram, (c) ground-truth, (d) Otsu method (T = 173), (e) Ridler method (T = 172), (f) Kapur method (T = 25), (g) Tsai method (T = 133), (h) Ng method (T = 145)

2.5 Dedicated Algorithms for Defect Detection in Thermal Image

Previous section has discussed the algorithms for image segmentation in the sense of image thresholding. As already shown by examples, these algorithms do not work well when applied to thermal images for segmentation purpose. Due to this reason, dedicated algorithms for thermal image segmentation have been proposed. Similar to visible image application, the purpose of thermal image segmentation is commonly to separate object of interest from its surroundings. Often, the object in this thermal image the *warm* or bright object.

Few efforts have been devoted to detect defect as depicted in a thermal image. Some methods use the thresholding technique for the detection, and others employ other criterion.

Minor and Sklansky (1981) proposed a method for extracting blobs in infrared images. The intensity of the original image was normalized into certain range, then the mean of this image was obtained. Other procedures such as edge detection, spoke filtering and segmentation of blobs were applied for segmentation process.

Hamadani (1981) employed a first order statistics properties, mean μ and standard deviation σ, to extract a *warm* object in a thermal image. The threshold level is given by:

$$T = k_1 \times \mu + k_2 \times \sigma \tag{2.20}$$

where $\mu = \frac{1}{M \times N} \sum_{i=1}^{M} \sum_{j=1}^{N} f(i,j)$, $\sigma = \sqrt{\frac{1}{M \times N} \sum_{i=1}^{M} \sum_{j=1}^{N} (f(i,j) - \mu)^2}$, and $k_1 = k_2 = 1$ for typical low-resolution thermal images. For higher resolution $k_1 = 1$ or $k_1 = 1.5$ and $k_2 = 2$ may yield better results (Ritter and Wilson, 2001).

This algorithm is not automatic, since the constants k_1 and k_2, which are image type dependent, should be determined manually (supervised approach or need a human intervention). Figure 2.7 shows the detection result using this algorithm for various k_1 and k_2. After doing some testing (and as also confirmed by Figure 2.7), the

constant k_1 has great impact on the thresholding result. Therefore, to successfully detect defects by this algorithm, one should adjust this value properly. But it is worthy to note that this adjustment should be done carefully, since if the first term of the right-hand side in Equation (2.18) is over adjusted, the T value will be greater than 255 and thus fail for an 8-bit image.

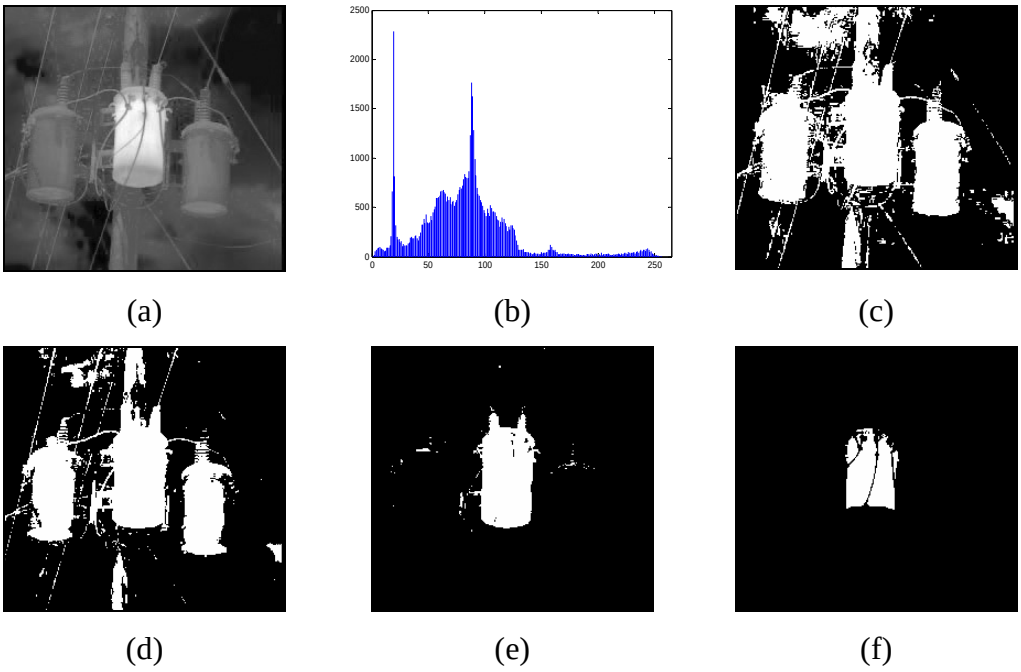

Figure 2.7 (a) Thermal image and (b) its histogram, thresholded with (c) k_1 = 1, k_2 = 1, T = 90, (d) k_1 = 1, k_2 = 2, T = 100, (e) k_1 = 1.5, k_2 = 1, T = 132, (f) k_1 = 2, k_2 = 1, T = 172

Maldague *et al.*, (1990) developed two step algorithms for defect extraction in thermal images. Firstly, the locations of the defects (seeds) are found. Secondly, a specific threshold is obtained for each of the defects detected by region-growing around those seeds.

For one defect located at (x,y) in the image f, the threshold is first set to $T = f(i,j)$ and the number of neighboring pixels n around T agglomerated together and having the same brightness T. The process is repeated until an image boundary is hit. It was noticed that often a sudden increase in the number of pixels was present in n when the background was reached. Since this number of pixels is generally greater

than what is obtained by manual segmentation, the threshold level is then corrected to:

$$T = 1/\sqrt{2} \times T \tag{2.21}$$

In its implementation (Maldague, 1993), (Maldague, 2001), the user should determine number of desired seeds (defects) to be detected and also the distance (in pixels) among these seeds. Hence, as Hamadani's method this technique is not fully automatic. Figure 2.8 shows the defect detection (crosshair) by this algorithm. This figure is obtained by determining five seed points with distance 50 pixels for each seed in Figure 2.8(a) and distance 100 pixels for Figure 2.8(b).

(a) (b)

Figure 2.8 Defect detection by Maldague's technique

Araki *et al.*, (1993) used *fuzzy c-means* clustering algorithm (Bezdek, 1981) to segment occupants in a room from a thermal image. Fuzzy c-means was applied first to remove the background, and then *peak-climbing* algorithm (Khotanzad and Bouarfa, 1990) was used to identify the number of occupants, followed by a *region growing* algorithm for accurate segmentation. It used three main algorithms in the segmentation process; hence its cost was expensive from the time processing perspective.

Chang *et al.*, (1997) generalized Olivo's method (Olivo, 1994) by means of dilated wavelet for automatic multi-level thresholding. In this technique, image is first convolved with dilated wavelet set. *Beginning of a peak* of this histogram is indicated by positive crossover of a zero-crossing. *Ending of a peak* is represented by negative crossover of a zero-crossing. The threshold value is considerably located either to the right of a negative crossover or to the left of a positive crossover. To get a best segmentation result for a single scale, a cost function has been derived in which the minimum cost function is the best scale for multi-level thresholding.

Darabi (2000) and Darabi and Maldague (2002) developed an algorithm for defect detection based on neural network. The neural network was trained with defective patterns of simulated data. The architecture with 30 neurons in input layer, 15 neurons in hidden layer, and 1 neuron in output layer was designed for this purpose. They showed a 96.8% correct classification of the network.

Parsi and Parsi (2001) proposed an algorithm for thermal image object extraction using the seed paradigm similar to that as proposed by Maldague *et al.* (1990). The seed was determined by the maximum gray level in the image. Then, they drew a cross of *N* pixels long from the seed in the four direction top, bottom, left, and right. Along each of the *4N* directions, they looked at the gray level profile and marked three places where the gray level value dropped most significantly. The determination of the threshold is done by finding consensus among thermal gaps. The optimum threshold is where the gray level value contains the largest number of gaps.

Šapina (2001) computed six textural features (Haralick *et al.*, 1973), (Haralick, 1979), (Baraldi and Parmiggiani, 1995) based on gray level co-occurrence (GLCM) matrix (Haddon and Boyce, 1990), (Haddon and Boyce, 1993) to extract the warmest object from its background.

Figure 2.9 shows the result by employing Sapina's technique for six textural features (maximum probability, energy, contrast, inverse difference moment, correlation, and variance) of GLCM based thermal image. From the figure, it seems that the variance feature has the good candidate as a defect detector. However, it still needs other algorithm to really separate defects from its background.

From the time processing perspective, after some experiments and even by reducing the gray level into 64 levels, it was found that this technique is still time consuming. To calculate the variance feature, it took 66.18 seconds on Pentium® 4, 1.90 GHz and RAM 512 MB. Compared to Hamadani's algorithm (0.45 seconds) and Maldague's algorithm for 10 seeds (0.46 seconds) for detection with the same image and on the same machine, variance feature technique is considerably too slow.

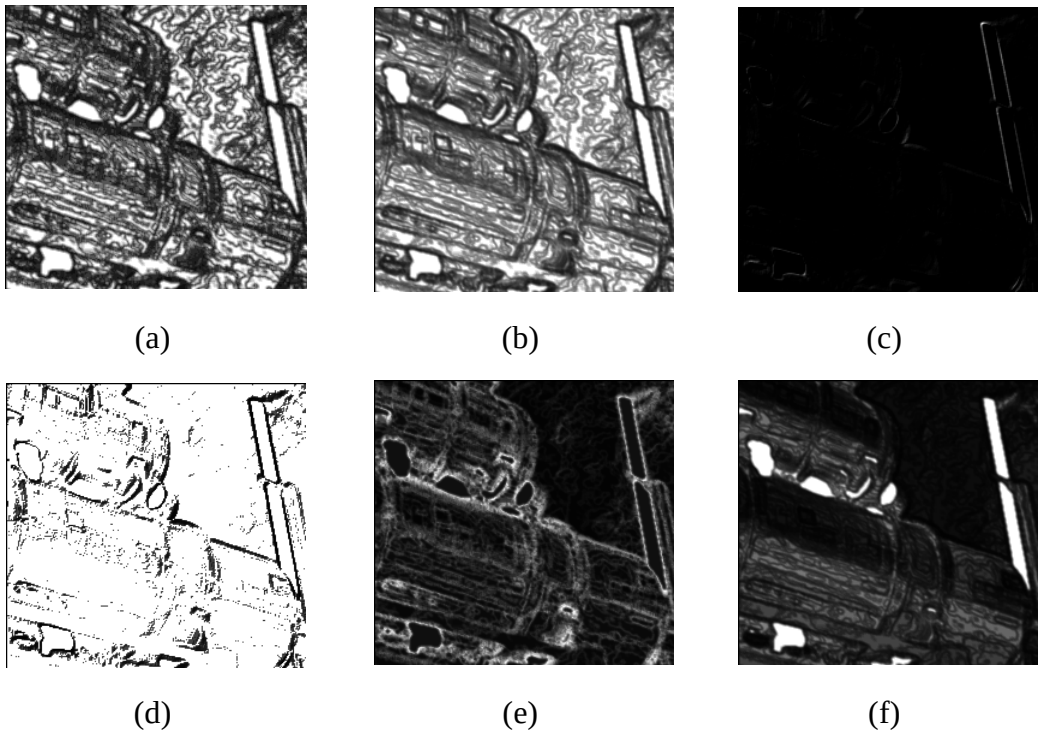

Figure 2.9 Sapina's technique for six textural features: (a) maximum probability, (b) energy, (c) contrast, (d) inverse difference moment, (e) correlation, (f) variance

Jin (2004) presented a segmentation technique for thermal image based on fuzzy filtering, the criteria of maximum entropy (Kapur *et al.*, 1985) and intelligent genetic algorithm. This algorithm is quite complex and not easy to implement.

Wu *et al.* (2004) combined a 2-D histogram of the image with standard fuzzy *c*-means (FCM) algorithm. The method for reducing computation time was proposed by calculating matrix membership function. They claimed that their method was 82 times faster than the traditional FCM algorithm.

Silverman e*t al.* (2004) proposed a histogram based segmentation by compressing first the multi-dimensional information (typically spectral profiles) into single image data cube such as principal component images. A multi-dimensional histogram is then constructed; an analysis of the statistical distribution of the points makes it possible to segment the image based on the histogram extrema.

Omar (2005) and Omar *et al.* (2005) proposed a self-referencing method to detect seeds in a thermal image for active thermography. A seed defined as very small pixels in a thermal contrast image. It was not mentioned in their original document whether this technique will work for a non-seed (larger) defect.

Feng *et al.* (2005) employed particle swarm optimization (PSO) paradigm to accelerate 2-D entropy method for thresholding infrared image. The 2-D maximum entropy method is based on the 2-D histogram of the image. The 2-D histogram denotes the probability of gray-level value and its local average value respect to the size of the image. The 2-D histogram can be described with four quadrant areas where the first and second quadrant represent object and background, and the third and fourth quadrant represent edge and noise. The 2-D maximum entropy principle said that the determined threshold vector should make the first and the second quadrant have the maximum information. The exhaustive search by the 2-D entropy method takes too much time. The PSO method was then incorporated to speed up the searching process. The result showed some saving in the processing time.

Dufour (2005) detected defect by using edge detection technique. The longitudinal and transversal of defect profiles are detected with $g(x) = T(x+1) - T(x)$ and $g(y) = T(y+1) - T(y)$ respectively. This technique actually does not really isolate defect, a further process is needed to confirm area inside or outside the edges as defects.

Tao *et al.* (2007) segmented infrared objects using fuzzy entropy based on ant colony optimization (ACO) algorithm. Similar to PSO, ACO is an algorithm which is developed based on swarm intelligence (Bonabeau *et al.*, 1999). The best ant was selected from *K* initial ants to compute optimal threshold.

2.6 Defect Detection based on Local Intensities Operation

Local intensities operation (LIO) is a convolution operation using local window in which the pixel will be grouped into one class, either a group of bright pixels or dark pixels. LIO has two modes: local intensities weighting (LIW) and local intensities lighting (LIL).

Based on LIO paradigm, this report proposes two schemes for detecting defects in a thermal image. The specific application for these algorithms is for passive thermography, meaning that the detection is directly applied to the thermal image not to the derived thermal images (absolute contrast) which is the common case for active thermography.

In the first scheme, specific thresholding technique is proposed for defect detection. Three simple algorithms are developed: midway absolute thresholding, midway relative thresholding, and minimum frequency thresholding techniques. The discussion of these techniques is given in Chapter 3 and the experimental results are given in Chapter 4.

In the second scheme, the standard thresholding technique is employed to isolate the defect. Hence, in this scheme, it is not about developing a new thresholding algorithm; rather it deals with how to implement any thresholding techniques to a thermal image, something they are not designed for. Several global thresholding algorithms for visible image as described in the previous section will be tested for verification. Figure 2.10 shows the flowchart for defect detection based on LIO operation.

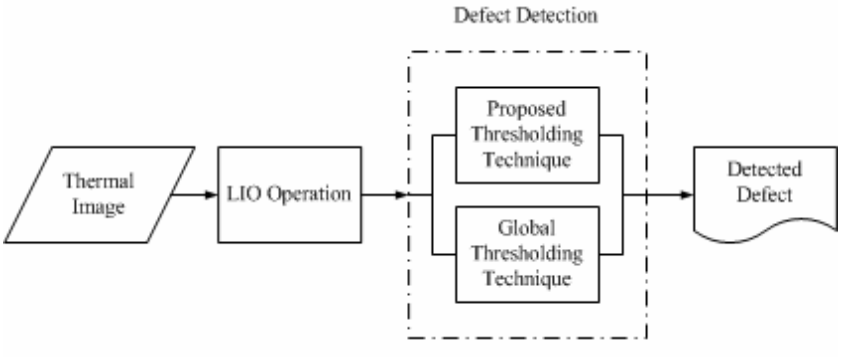

Figure 2.10 Defect detection based on LIO paradigm

CHAPTER 3

LOCAL INTENSITIES OPERATION AND MINIMUM FREQUENCY THRESHOLDING

3.1 Overview

Local intensities operation (LIO) is based on the idea of local neighborhood operation. LIO has two modes in its implementation. In the first mode, LIO will brighten the bright area and darken the dark area. In this mode, the operation is called as *local intensities weighting* (LIW). In the second mode, the opposite action is performed, LIO will brighten the dark area and darken the bright area. This is called as *local intensities lighting* (LIL) operation.

In LIW, it is assumed that the defect is the brightest area, and the background or sound area is the darkest area. On the contrary, LIL assumes that the darkest area is the defective area while the brightest area is the sound area.

After pre-processing with the LIO operation, LIO image then need to be thresholded so that the background and the defect areas are separated. Simple *midway absolute thresholding* (MAT), *midway relative thresholding* (MRT), and *minimum frequency* (MFT) thresholding techniques are proposed for this purpose.

3.2 Theoretical Foundation

Consider a pixel $f(i,j)$ in a thermal image with its 8-connectivity configuration as shown in Figure 3.1, where $z1 = f(i-1,j-1)$, $z2 = f(i-1,j)$, $z3 = f(i-1,j+1)$, $z4 = f(i,j-1)$, $z5 = f(i,j)$, $z6 = f(i,j+1)$, $z7 = f(i+1,j-1)$, $z8 = f(i+1,j)$, and $z9 = f(i+1,j+1)$.

LIO operator is defined as in Equation (3.1). For LIW operation, α = z1*z2*z3*z4*z5*z6*z7*z8*z9, and β = 1. For LIL operation, α = 1, and β = z1*z2*z3*z4*z5*z6*z7*z8*z9. By substituting these variables, both operators can be written in the form as in Equations (3.2a) and (3.2b).

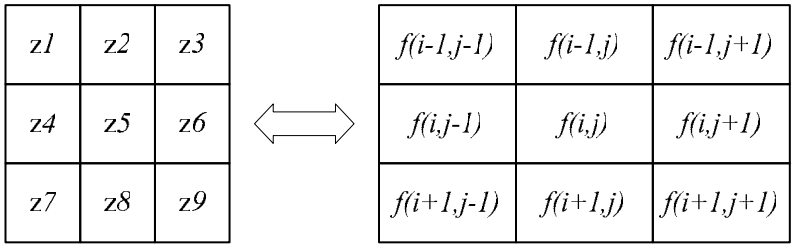

Figure 3.1 LIO window

$$\mathrm{LIO} = \frac{\alpha}{\beta} \tag{3.1}$$

$$\mathrm{LIW} = z1 * z2 * z3 * z4 * z5 * z6 * z7 * z8 * z9 \tag{3.2a}$$

$$\mathrm{LIL} = \frac{1}{z1 * z2 * z3 * z4 * z5 * z6 * z7 * z8 * z9} \tag{3.2b}$$

Figure 3.2 illustrates the LIO operation. This is done through out the entire image as a convolution process. The pixel values are then normalized by dividing with the maximum pixel value.

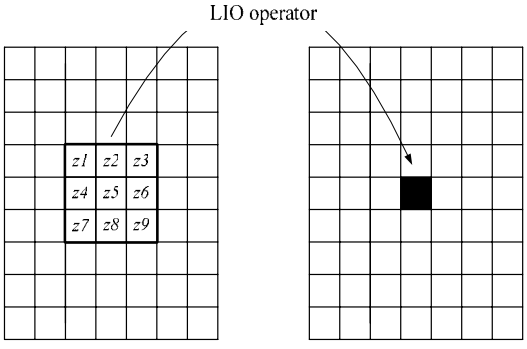

Figure 3.2 Local intensities operation

This process is repeated until most pixel values concentrate only in the darkest and brightest area. In practice, LIW has some levels of operation. The first LIW operation to the original thermal image is called as the *1st level* LIW, the next LIW operation onto this 1st level LIW will be called as the *2nd level* LIW, and so forth.

But not as LIW, LIL has only one level. This level will highlight the dark pixels and change the intensities into bright pixels. The bright pixels will be changed to the dark pixels. The defect is now represented by bright pixels. If it is still desired to emphasize this defect, the successive LIW operation can be applied then.

Figure 3.3 shows a thermal image after 4th–level LIW operation. As shown in the figure, image histogram of the original thermal image is multimodal. At this stage, it is quite difficult to separate between the object (defective area) and the background (sound area). After applying the 1st level LIW, most pixels are then shifted to the dark region and image histogram tends to have a unimodal representation. After the subsequent levels, most dark and most bright pixels have the highest pixel counts (refer to Figure 3.3).

Other property of LIW which is crucial to note is that at every level, LIW operation tends to shrink the shape of the defect. This is due to the nature of how the LIW image is being computed (see Equation 3.2a). Figure 3.4 illustrates this situation. If it is desired to keep the shape of the defect, a successive morphological operation (dilation) (Giardina and Dougherty, 1988) can be applied after applying every LIW operation.

Figure 3.5 shows both the LIL operation as well as the LIW operation for comparison. This figure shows clearly the difference between LIW and LIL operations. It is also obvious (as stated before) that LIL operation will brighten the dark area and darken the bright area.

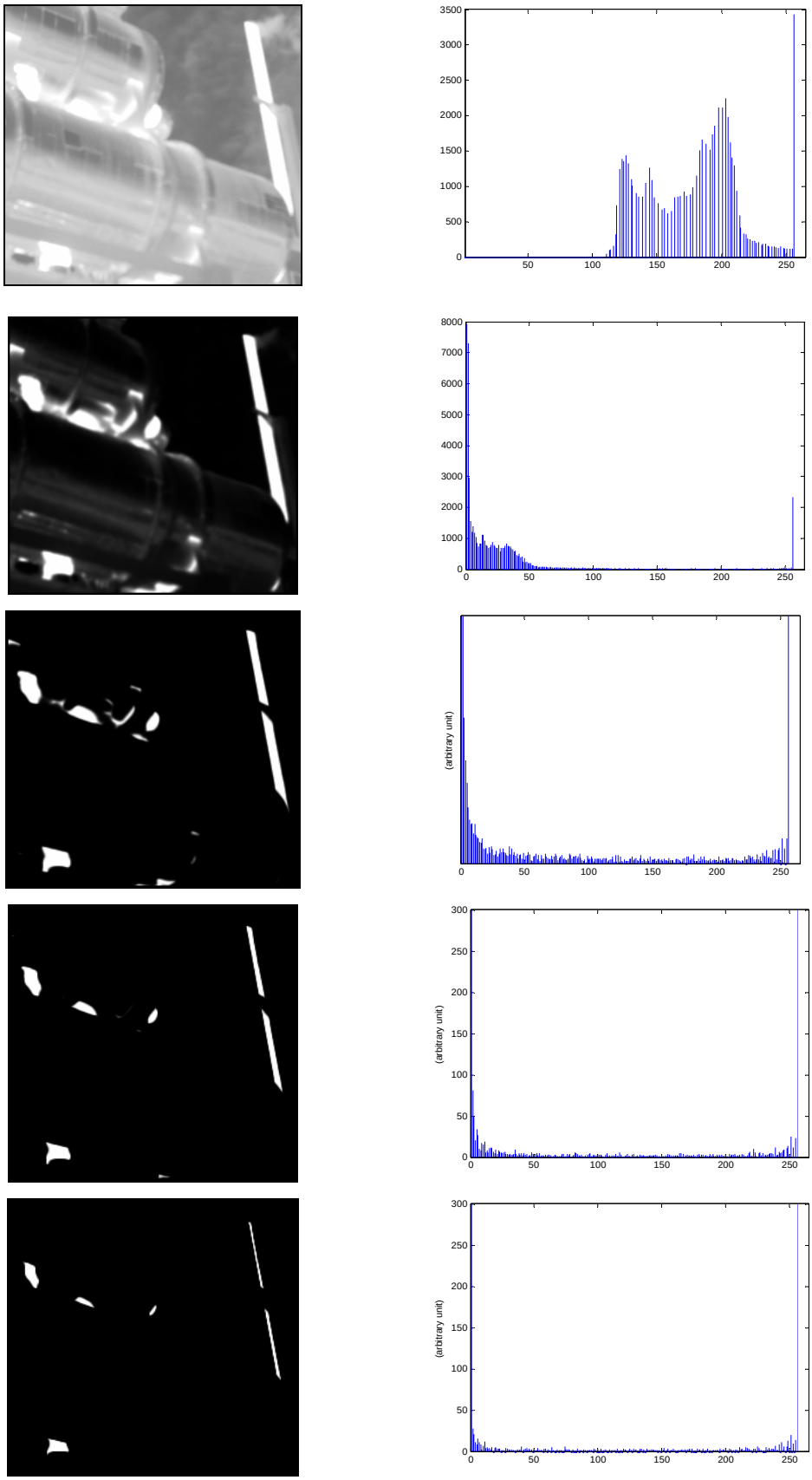

Figure 3.3 (from top to bottom): original thermal image and its 1st to 4th level LIW image along with its histogram

(a) (b) (c)

Figure 3.4 Shrinking effect of the LIW operation (from left to right): (a) 3rd level LIW, (b) 4th level LIW, (c) subtract (*a*) from (*b*) shows the shrunk edge

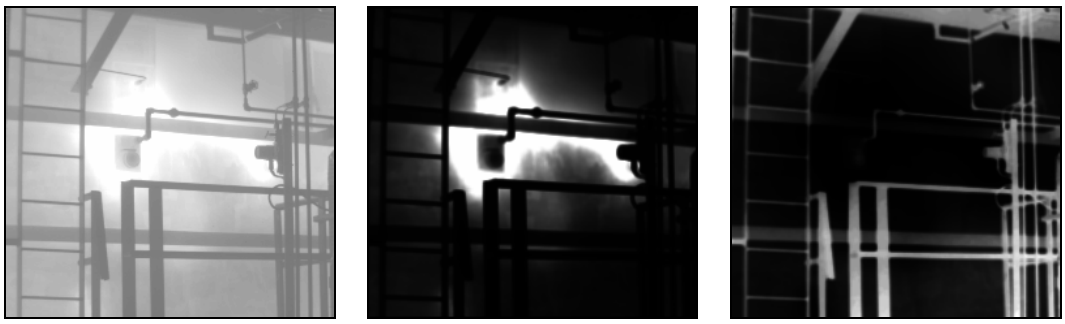

(a) (b) (c)

Figure 3.5 (a) Grayscale thermal image, (b) 1st level LIW, (c) LIL image

3.3 Practical Implementation

In both LIW and LIL operations, pixel intensities are forced to concentrate on the high and low levels only. LIW operation is designed to detect *hot* defect only while LIL operation is to detect *cold* defect only.

In order for LIW and LIL operations to have the capability for detecting both defect types (hot and cold defects), the following procedures can be applied:

1. Apply LIW operator onto the original thermal image $f(i,j)$ to obtain $g(i,j)$.
2. Apply LIL operator onto the original thermal image $f(i,j)$ to obtain $h(i,j)$.
3. Add together both images $g(i,j)$ and $h(i,j)$.

Figure 3.6 shows the implementation of these procedures. The effect of both LIW and LIL operations in shrinking edges is clearly shown in the resulting image. Thus, before the addition operation, morphological dilation may be applied to reduce this effect.

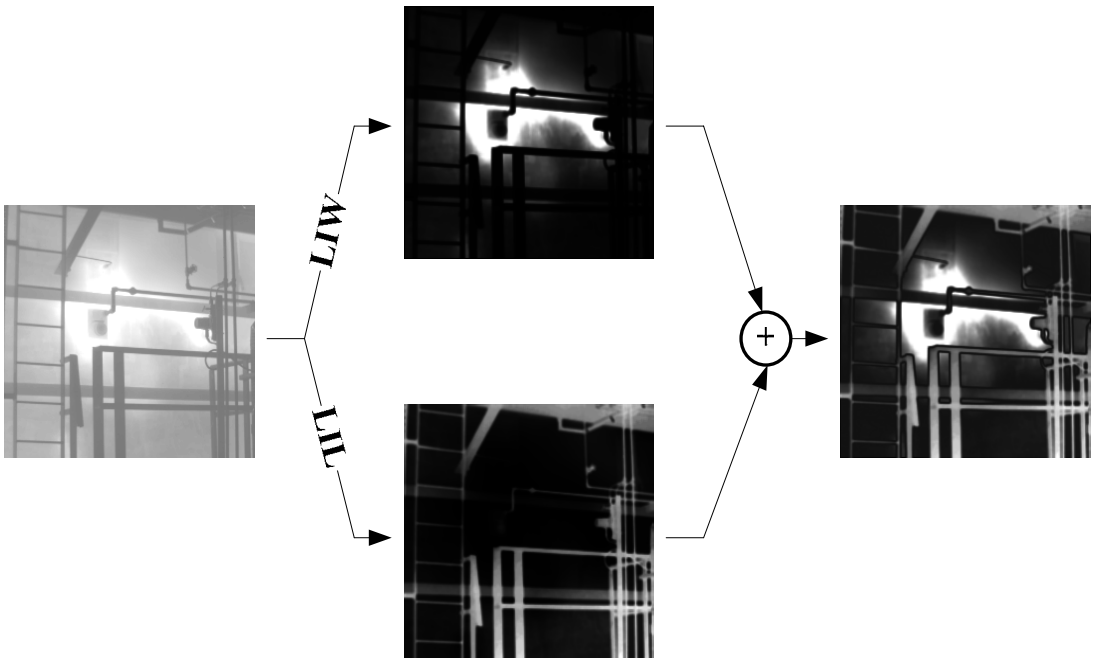

Figure 3.6 Procedures to detect both hot and cold defects

3.4 MAT, MRT, and Minimum Frequency Thresholding

After applying LIO operation in a thermal image, most pixels are now concentrated only in a dark and bright regions. The pixels distribution in between has a uniform-like distribution after applying 2nd–level LIW operation (Figure 3.7). This report proposes three strategies to segment the defect from the background:

Midway absolute thresholding (MAT) – threshold value using this technique is calculated by obtaining the halfway value between minimum and maximum gray-level used in the image histogram. If gray-level is $i = 0 \ldots L$, then MAT is defined as:

$$T = \text{round}\left[\frac{L-0}{2}\right] \tag{3.3}$$

It is clear from Equation (3.3) that if full range gray-level is used in LIO image, then for an 8-bit color system, *T* will always be 128.

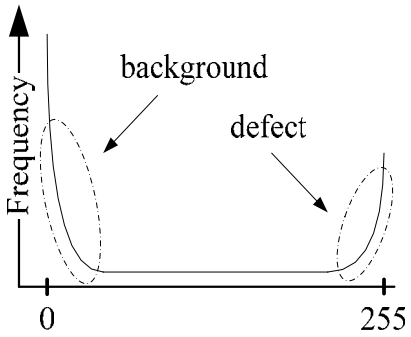

Figure 3.7 Gray-level distribution after LIO operation

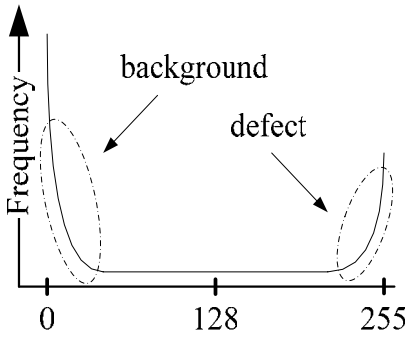

Figure 3.8 Midway absolute thresholding concept

Midway relative thresholding (MRT) – the threshold value as in Equation (3.4) is obtained from the average value of pre-determined minimum gray-level T_{min} with maximum gray-level T_{max}:

$$T = \text{round}\left[\frac{T_{\max} - T_{\min}}{2}\right] \tag{3.4}$$

T_{min} and T_{max} values can be determined *manually* by user selection or *automatically* by using *histogram gradient* of gray-level value. Histogram gradient is derived from the following equations:

$$r(i) = h(i+1) - h(i) \tag{3.5}$$

where $h(i)$ is image histogram at gray-level i. Performing this histogram gradient will invert the corner of the dark region as shown in Figure 3.9. Then from this histogram gradient graph, T_{min} and T_{max} is determined by:

$$T_{\min} = r(i) \quad \text{if } r(i) > r(i-1) \text{ AND } r(i) > r(i+1) \text{ AND } r(i) \geq 0 \tag{3.6a}$$

$$T_{\max} = r(i) \quad \text{if } r(i) < r(i-1) \text{ AND } r(i) < r(i+1) \tag{3.6b}$$

for time efficiency, T_{min} search starts from gray-level $i = 0$ to $i = L$ while T_{max} search starts from $i = L$ to $i = 0$. The searching process is stopped once the above criteria are satisfied.

It is clear from Equations (3.6a) and (3.6b) that if T_{min} and T_{max} are the minimum and the maximum gray-level values in the image histogram respectively, then this is the special case for MAT thresholding.

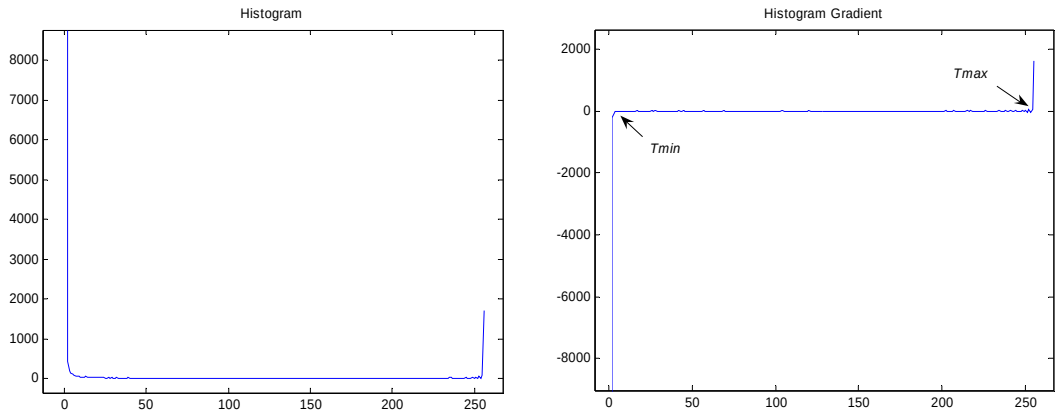

(a) (b)

Figure 3.9 Midway relative thresholding concept: (a) histogram, (b) histogram gradient

Minimum frequency thresholding (MFT) – the third thresholding scheme proposed for detecting defect in LIO image is based on the minimum gray-level frequency.

Based on experiments, it is found that *the most-left* of minimum gray level frequency will give a good thresholding result. This theory is laid on the assumption that, for the case of hot defect, the centroid of the defect usually always has the brightest intensity, and this intensity gradually becomes lower towards the defect boundary. Abrupt changes from gray-level i to $i–n$, n = 1, 2, 3, …, i, or discontinuities that occur indicate this boundary.

The most-left minimum gray-level value in image histogram is selected as the threshold value (Equation 3.7) by assuming that if there is gray-level continuity in image histogram in the left of the most-left, meaning that these gray-level values indicates image background. Figure 3.10 illustrates the concept of MFT.

$$T = \min\{T_i\} \quad \text{if } i = 1...N \quad \text{then } i = 1 \tag{3.7}$$

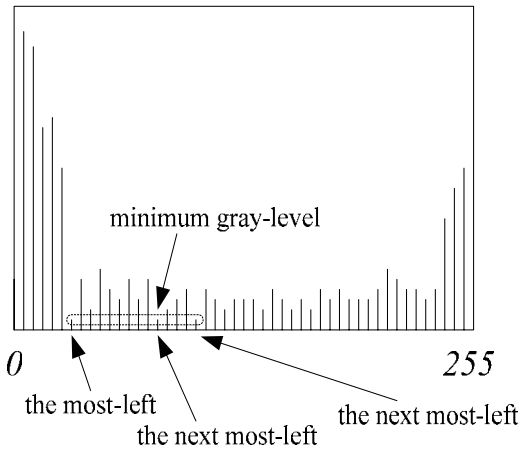

Figure 3.10 Minimum frequency thresholding principle

CHAPTER 4

EXPERIMENTAL RESULTS AND DISUCUSSION

4.1 Overview

This chapter shows the experimental results and their discussion. The developed algorithms are evaluated and compared with existing algorithms for defect detection. The standard evaluation measure is used for this comparison validity.

4.2 Thermal Image Dataset

All thermal images were taken from real world petrochemical plant equipments or facilities. In collaboration with MTBE Malaysia Sdn. Bhd. (subsidiary of Petronas Sdn. Bhd.), Gebeng, Kuantan, Pahang, thermal images were obtained from their site.

Twelve thermal images are used for testing the developed algorithms and their comparison with other existing techniques. All of these thermal images represent *hot defect*, as shown in Figure 4.1(a) – (l). These images were taken when the objects were being in-operation. Thermal infrared camera Inframetrics PM 390 (see Appendix 1 for details specification) was used for capturing these images. These thermal images represent various gray-level distribution types. Figure 4.1(j) represents *unimodal* distribution. This type is difficult to segment, even the standard Otsu thresholding algorithm will fail for such type of images (Kittler and Illingworth, 1986). Figure 4.1(b), -(g), and -(h) represents image with *bimodal* distribution. Most of existing algorithms for segmentation or defect detection were designed to work well on this type of distribution. Other thermal images represent *multimodal* gray-level distribution which is the most difficult to segment. Further algorithms are needed to successfully segment this type of image.

4.3 Experiments with MAT, MRT, and MFT Techniques

In this section, MAT, MRT, and MFT techniques that already presented in the previous section are tested. Thermal image dataset for hot defect (Figure 4.1) is used.

Before applying these algorithms, LIO operation needs to be applied onto the original thermal image as pre-processing step. Since hot defect is to be detected, LIW operator is used. As already discussed and shown in Chapter 3, although LIW operation can be applied successively to generate *n*-level LIW image, but in this experiment, only the first two levels LIW operation is applied since upto this level the detection result gave a good result. Figure 4.2 and Figure 4.3 show the 1^{st} and 2^{nd} level LIW operation onto these original grayscale images.

Figure 4.4, -4.5, -4.6, -4.7, -4.8, and -4.9 show the segmentation results when applying MAT, MRT, and MFT thresholding on the 1^{st} and 2^{nd} level LIW images respectively. From these figures, it can be seen that at the 1^{st} level LIW, MAT and MRT give quite similar results but mainly with false-positive. Note that at this level, MFT technique gives a better result. At 2^{nd} level LIW, MAT, MRT, and MFT techniques give the same result, but again as before MFT technique is superior to the other two. The performance of these techniques is discussed in the next section.

4.4 Comparative Study and Performance Evaluation

To compare the proposed algorithms and evaluate their performance, comparative study has been done. Nine existing algorithms (five non-dedicated algorithms and other four dedicated algorithms designed for defect detection in thermal image) were selected for comparison purpose.

For non-dedicated algorithms, this report compares each algorithm from five categories as proposed by Sezgin & Sankur (2004), i.e. Rosenfeld algorithm (Rosenfeld & De la Torre, 1983) for shape category, Otsu algorithm (Otsu, 1979) for cluster category, Kapur algorithm (Kapur *et al.*, 1985) for entropy category, Tsai algorithm (Tsai, 1985) for attribute category, and Abutaleb algorithm (Abutaleb, 1989) for spatial category. It is worthy to note that although Kittler cluster algorithm

(Kittler & Illingworth, 1986) was confirmed as the best algorithm by previous research (Sezgin and Sankur, 2004), after some experiments it was found that this algorithm for most thermal image dataset failed to give meaningful result. Therefore, Otsu algorithm was selected as representation of cluster category by considering its popularity and easy to implement.

For dedicated algorithms, four methods were selected: Hamadani algorithm (Hamadani, 1981), Olivo algorithm (1994), Sapina algorithm (Sapina, 2001), and Sezgin algorithm (Sezgin and Sankur, 2003). The selection was based on its automatic property and its ability to segment defects. Note that for Sapina algorithm, since it does not really isolate the defect, the highest pixel value in the processed image is considered as the defective pixels.

It is not easy to compare one segmentation method to others (Yasnoff *et al.*, 1977). In this report, a simple *absolute error ratio* measure was used (Tao *et al.*, 2007). This measure is defined as the ratio between the absolute error, n_{diff}, and the total number of pixels N of an image:

$$r_{err} = \frac{n_{diff}}{N} \times 100\% \tag{4.1}$$

The absolute error n_{diff} is defined as the absolute difference in the number of object pixels between the ground-truth image with the tested image.

Figure 4.10 shows detection results using Otsu method (non-dedicated algorithm) and Figure 4.11 shows detection result using Hamadani method (dedicated algorithm) from dataset in Figure 4.1(a) to -4.1(l). It is clear from these figures that both methods (non-dedicated or dedicated algorithm) failed in detecting defects. Both methods tend to separate object (defect) and background uniformly.

As mentioned, LIW operation is actually designed as a pre-processing stage before the real detection algorithm is applied. To test the effectiveness of this operation, both the non-dedicated and dedicated algorithms were once again employed onto the LIW images for defect detection. Figure 4.12, -4.13, -4.14 and

-4.15 show detection result by Otsu and Hamadani techniques on the 1st and 2nd levels LIW image respectively. It is obvious that at 2nd level LIW, both non-dedicated and dedicated algorithm give outstanding results in segmenting defects.

The evaluation results (based on absolute error ratio) for all algorithms are given in Table 4.1. Table 4.2 shows the rank of these algorithms based on the average score of the measures. From Table 4.2, it is clear that by applying LIW operation, defect can be detected correctly whether it is detected using the simple proposed algorithm, dedicated, or non-dedicated algorithms. Although from this experiment, the 1st level LIW operation when combined with MFT algorithm gives the best result, actually this result indicates that the 2nd level LIW operation also give much better results for most cases.

This study also shows that for most cases, 2-D histogram based algorithm or gray-level co-occurrence matrix (GLCM) (as studied by Sapina) is better than 1-D histogram based algorithms even after applying LIW operation. But the main drawback of this method is its highly expensive computational cost (see discussion in Chapter 2).

Finally, Figure 4.16 shows the absolute error ratio for each tested thermal image for the 1st (MFT on 1st level LIW), the 11th (Otsu on the 1st level LIW), and the last rank (Tsai method on the original image thresholding). This plot indicates that Otsu and Tsai method cannot successfully detect a relative small defect.

Table 4.1 Performance of Defect Detection Algorithms

Approach		**Average Absolute Error (%)**
Technique	**Image**	
MAT	1st level LIW	4.20
MAT	2nd level LIW	1.50
MRT	1st level LIW	5.02
MRT	2nd level LIW	1.47
MFT	1st level LIW	0.91
MFT	2nd level LIW	1.53
Otsu	1st level LIW	15.90
Otsu	2nd level LIW	1.27
Hamadani	1st level LIW	15.43
Hamadani	2nd level LIW	1.36
Rosenfeld	Original	45.00
Otsu	Original	48.27
Kapur	Original	37.73
Tsai	Original	66.80
Abutaleb	Original	36.56
Hamadani	Original	28.79
Olivo	Original	53.14
Sapina	Original	1.78
Sezgin	Original	23.67

Table 4.2 Rank of Defect Detection Algorithms

Rank	Approach		Average Absolute Error (%)
	Technique	Image	
1	MFT	1st level LIW	0.91
2	Otsu	2nd level LIW	1.27
3	Hamadani	2nd level LIW	1.36
4	MRT	2nd level LIW	1.47
5	MAT	2nd level LIW	1.50
6	MFT	2nd level LIW	1.53
7	Sapina	Original	1.78
8	MAT	1st level LIW	4.20
9	MRT	1st level LIW	5.02
10	Hamadani	1st level LIW	15.43
11	Otsu	1st level LIW	15.90
12	Sezgin	Original	23.67
13	Hamadani	Original	28.79
14	Abutaleb	Original	36.56
15	Kapur	Original	37.73
16	Rosenfeld	Original	45.00
17	Otsu	Original	48.27
18	Olivo	Original	53.14
19	Tsai	Original	66.80

4.5 Detection of Cold Defects

The previous section shows the experimental result and its evaluation for detection of hot defect using the developed algorithms as well as comparison to other algorithms. LIW operation was employed for this hot defect type. This section is dedicated for detecting cold defect using LIL operation.

Figure 4.17 shows three thermal images along with its ground-truth and defect detection by using MFT on LIL image and Otsu method on original and on

LIL image respectively. It is obvious from these results that only after applying LIL operation defects can be detected correctly.

4.6 Summary

This chapter shows the experimental results and their discussions. It has been proven by experiments that by applying LIW operation a significance improvement for detecting defect has been achieved. For most cases, it has been found that the 1st level LIW operation before applying MFT algorithm for defect detection is sufficient. As for comparison, the 2nd level LIW has been experimented using MAT, MRT, and MFT. To further explore, one may extend to higher LIW levels and apply them using proposed thresholding algorithms or any thresholding algorithm whether it is designed for thermal images or not.

The previous section also shows that LIL operation works well for detecting cold defect which was fail if using other thresholding algorithms.

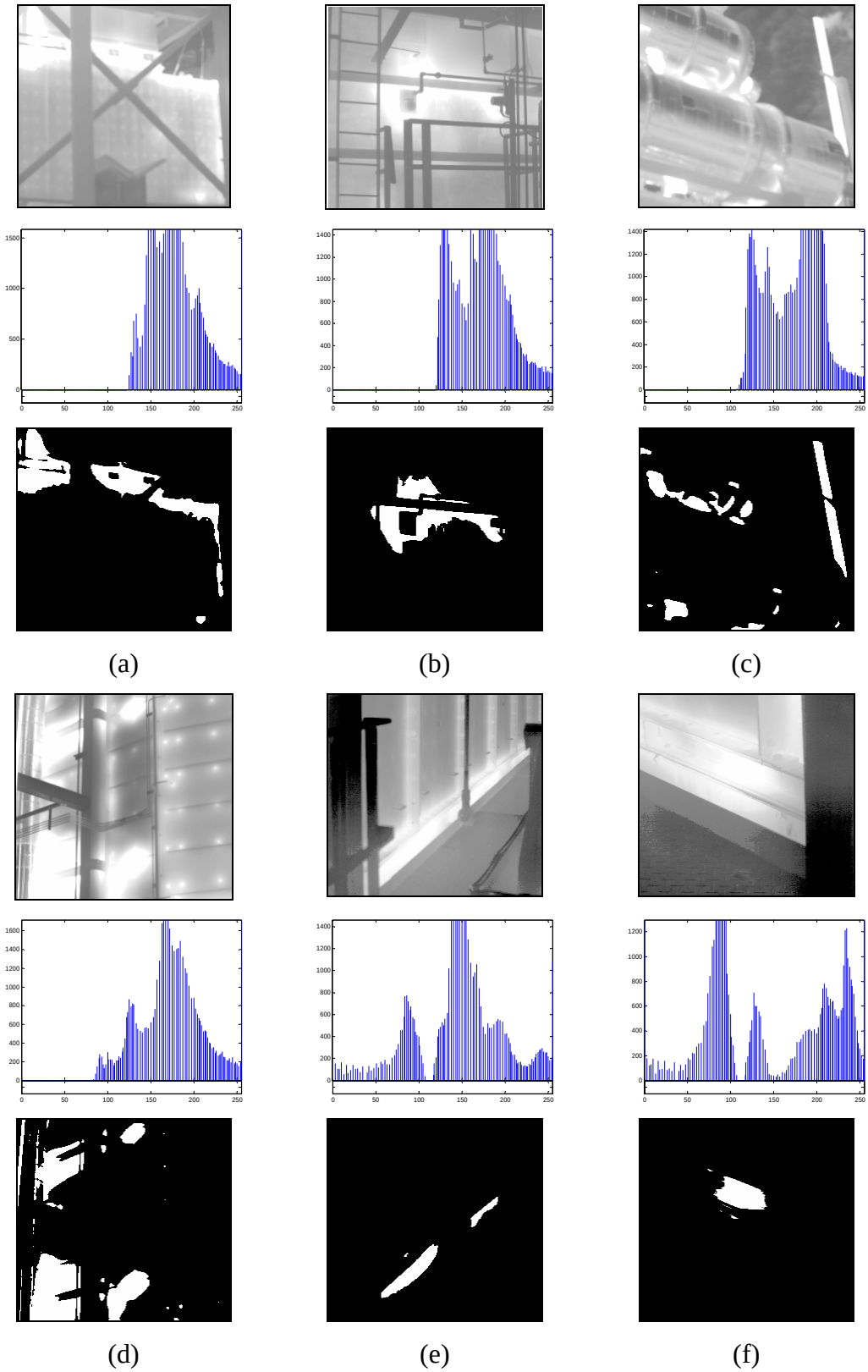

Figure 4.1 Thermal image dataset for *hot defect* with its histogram and ground-truth: (a) T = 243, (b) T = 245, (c) T = 243, (d) T = 252, (e) T = 250, and (f) T = 252

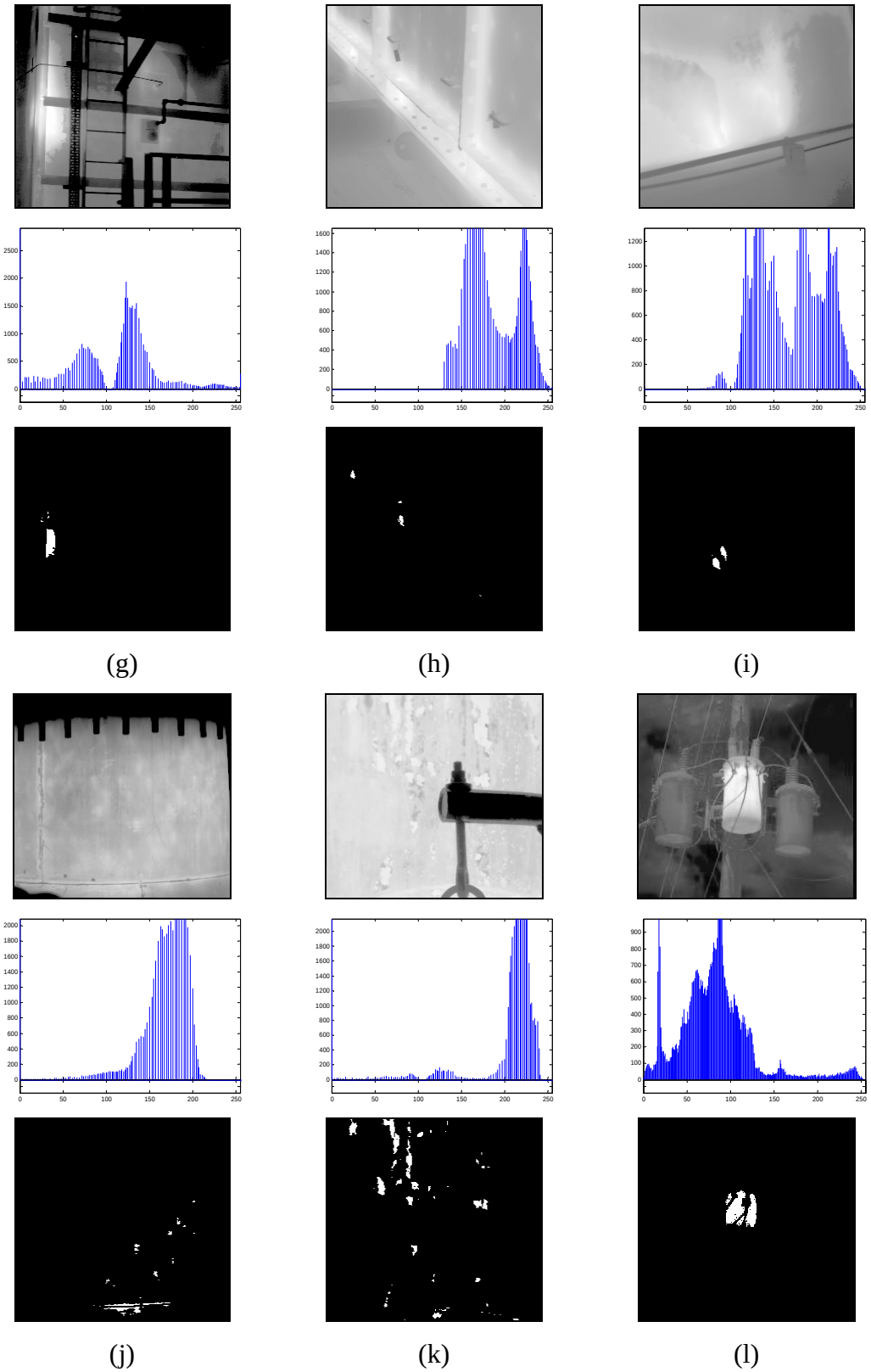

(g) (h) (i)

(j) (k) (l)

Figure 4.1 (cont.) Thermal image dataset for *hot defect* with its histogram and ground-truth: (g) T = 252, (h) T = 248, (i) T = 245, (j) T = 206, (k) T = 237, and (l) T = 233

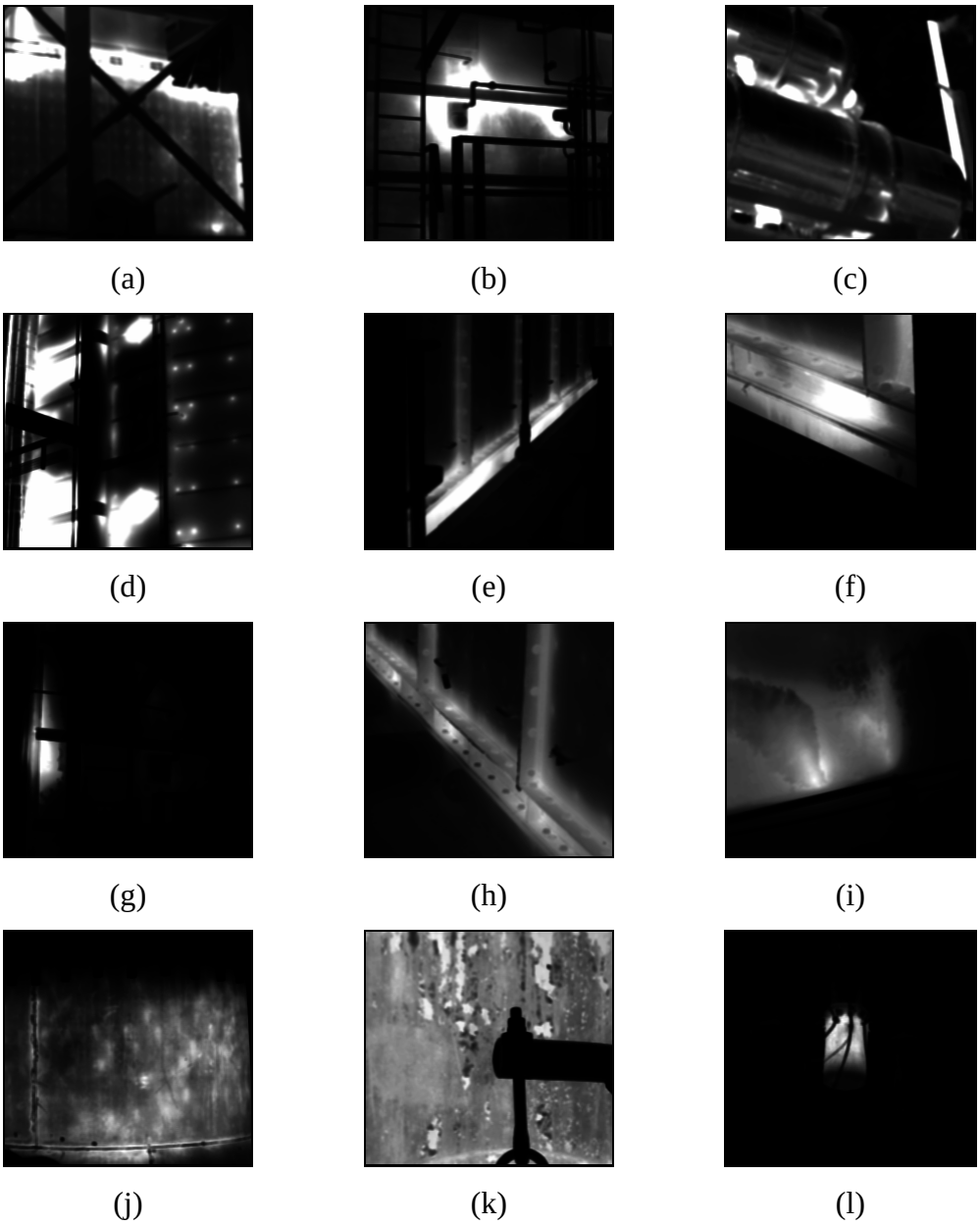

Figure 4.2 1st level LIW operation on thermal images consisting hot defect

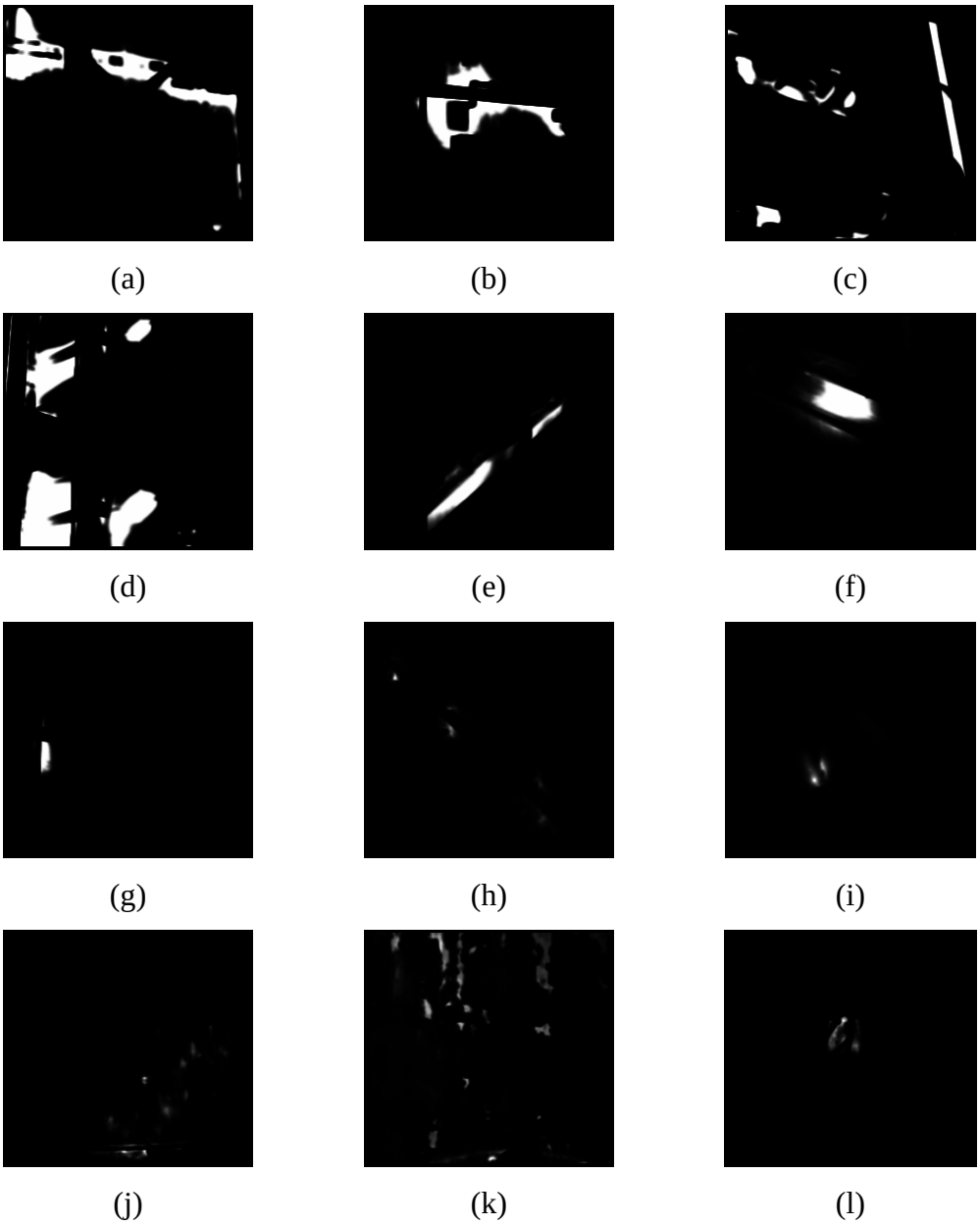

Figure 4.3 2nd level LIW operation on thermal images consisting hot defect

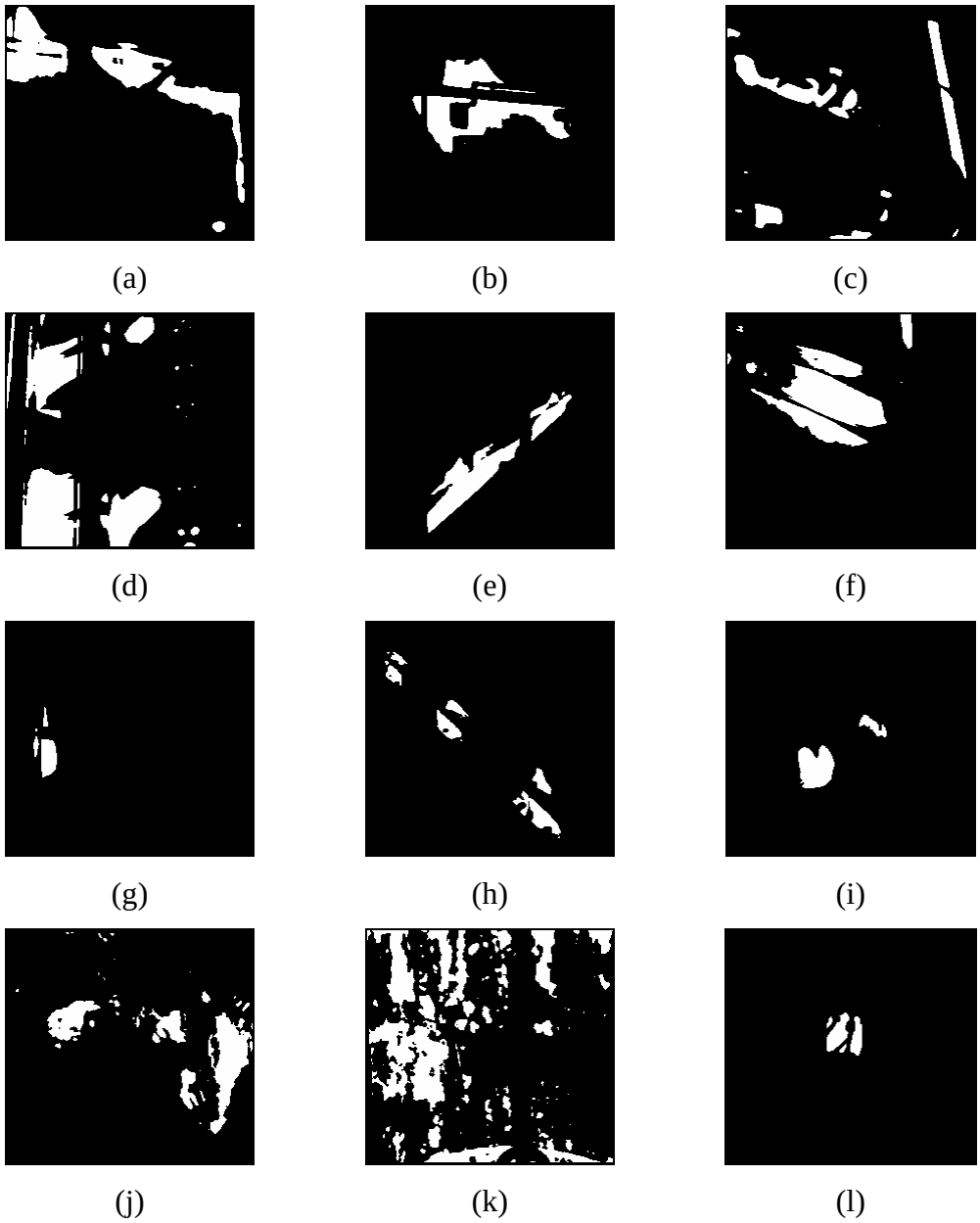

Figure 4.4 1st level LIW image thresholded with MAT algorithm: (a) to (l) $T = 128$

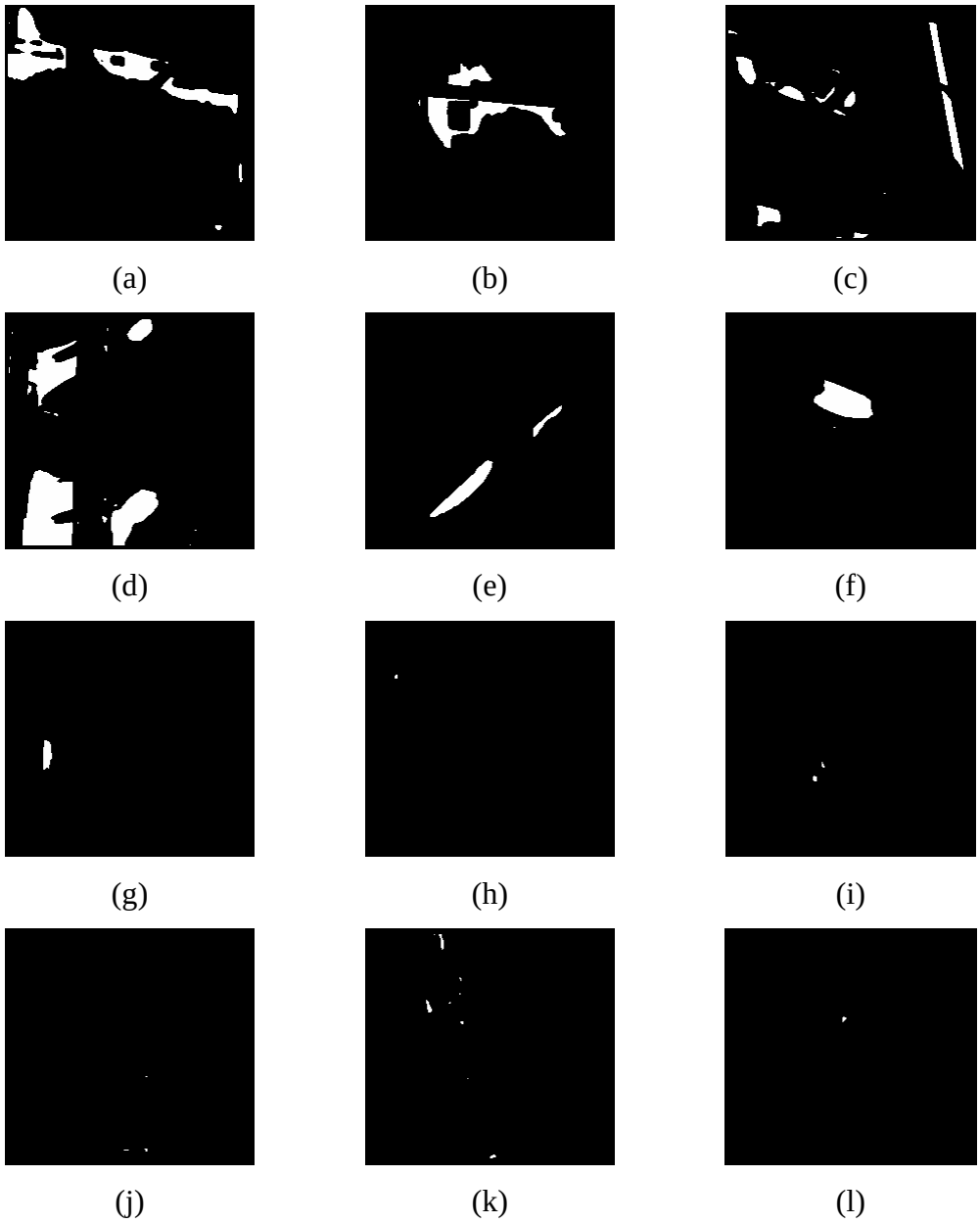

Figure 4.5 2nd level LIW image thresholded with MAT algorithm: (a) to (l) $T = 128$

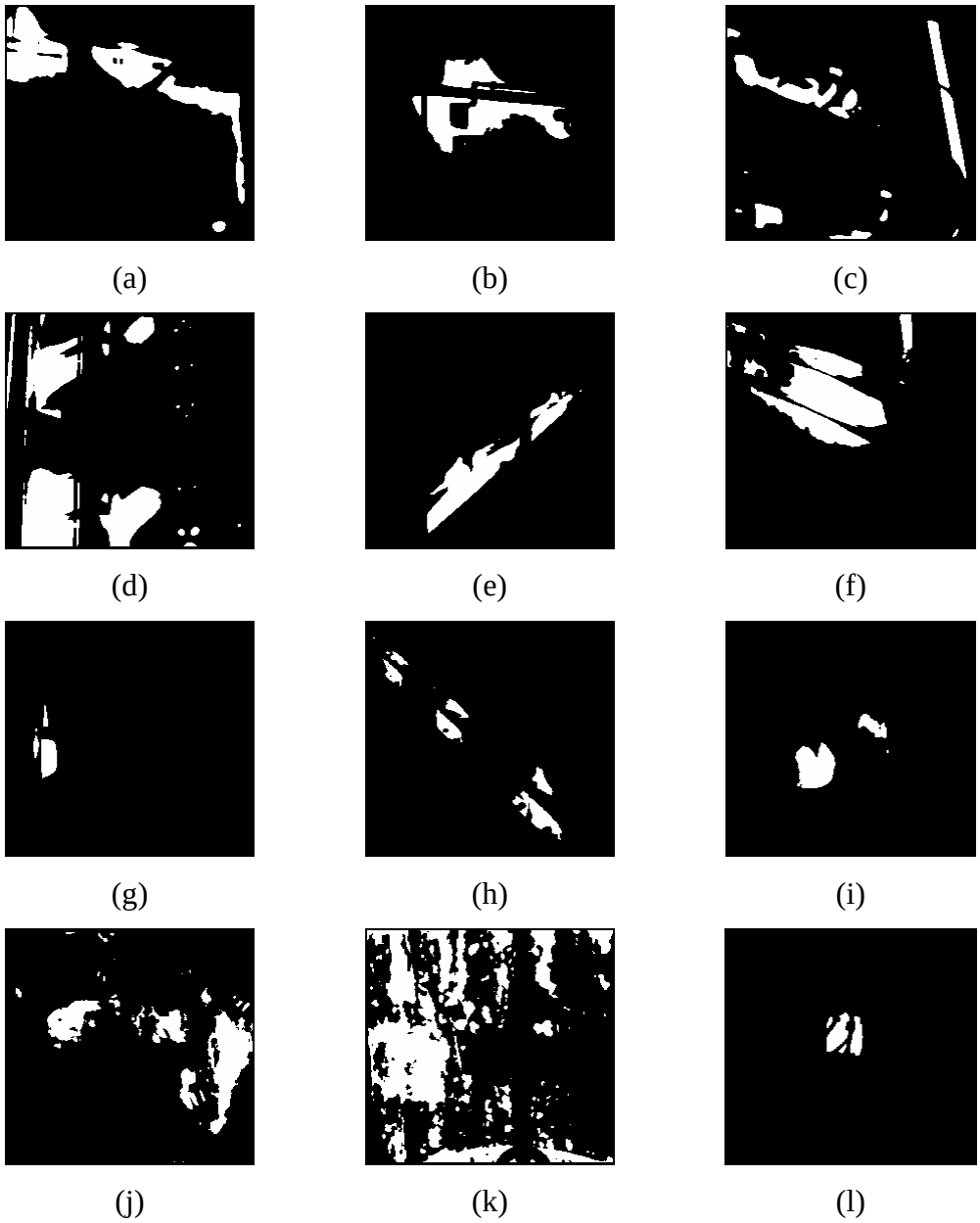

Figure 4.6 1st level LIW image thresholded with MRT algorithm: (a) T = 124, (b) T = 125, (c) T = 124, (d) T = 124, (e) T = 121, (f) T = 123, (g) T = 122, (h) T = 125, (i) T = 122, (j) T = 124, (k) T = 122, (l) T = 124

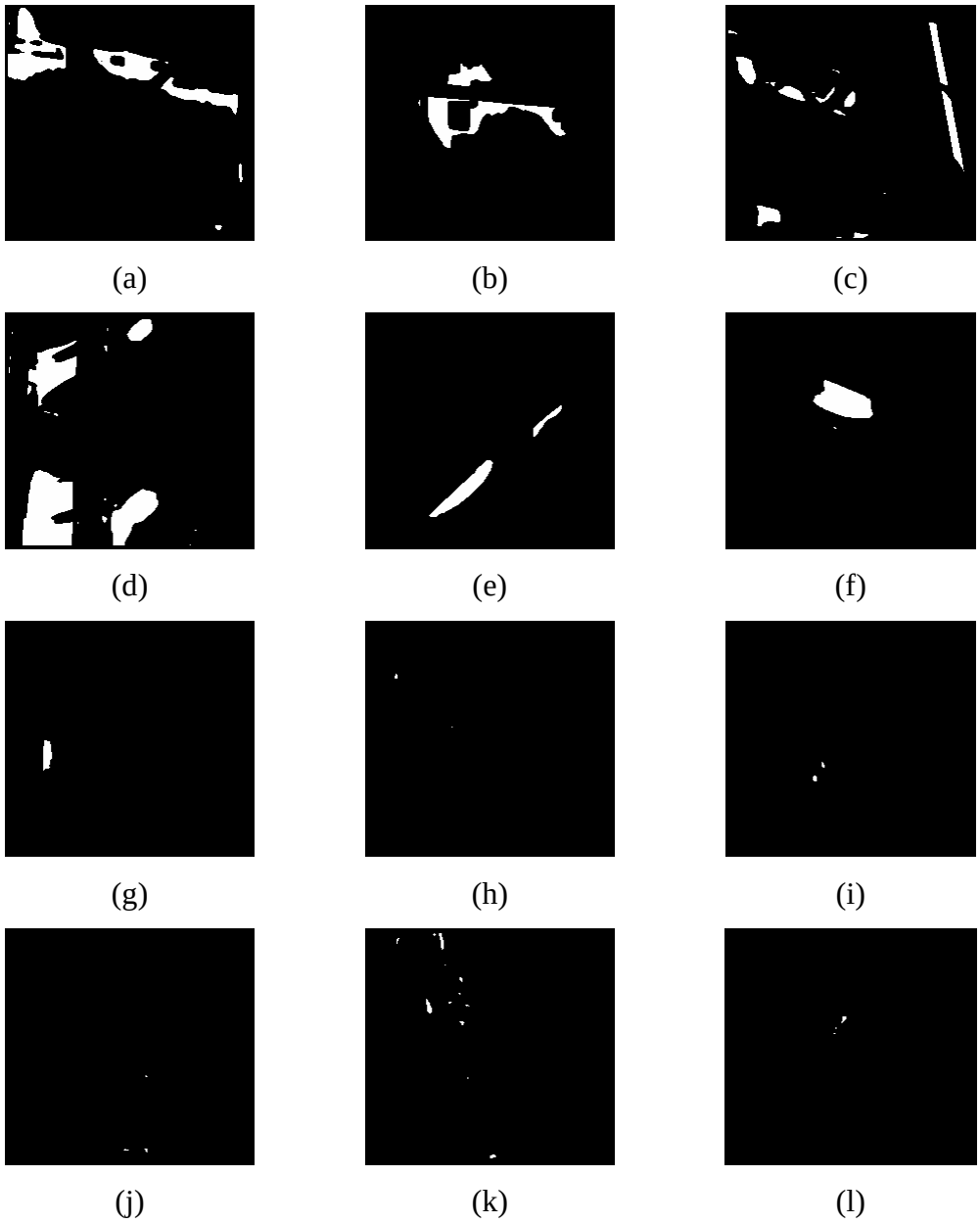

Figure 4.7 2nd level LIW image thresholded with MRT algorithm: (a) T = 121, (b) T = 118, (c) T = 123, (d) T = 124, (e) T = 123, (f) T = 122, (g) T = 123, (h) T = 115, (i) T = 124, (j) T = 118, (k) T = 115, (l) T = 106

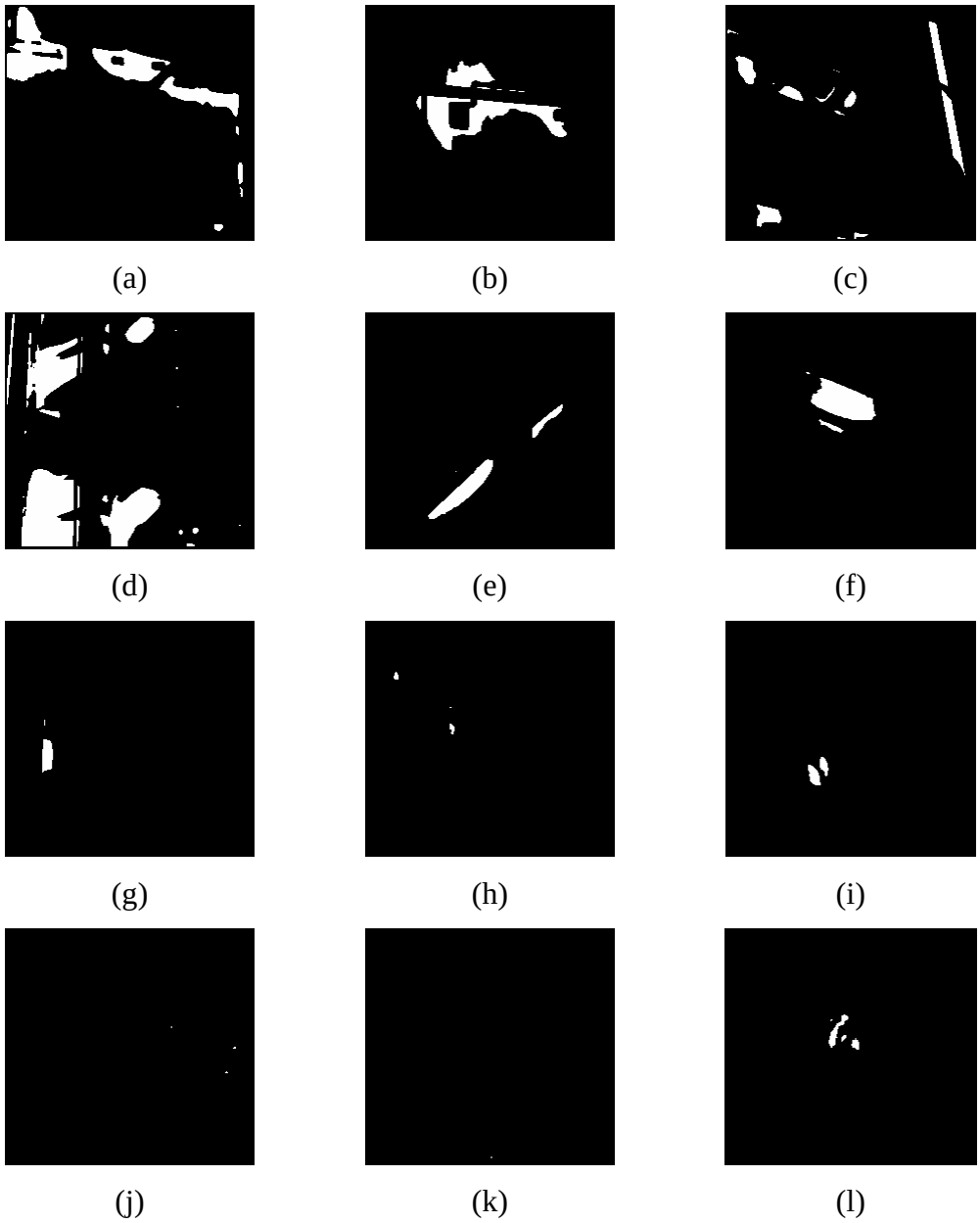

Figure 4.8 1st level LIW image thresholded with MFT algorithm: (a) T = 209, (b) T = 193, (c) T = 254, (d) T = 169, (e) T = 226, (f) T = 210, (g) T = 209, (h) T = 208, (i) T = 187, (j) T = 243, (k) T = 252, (l) T = 194

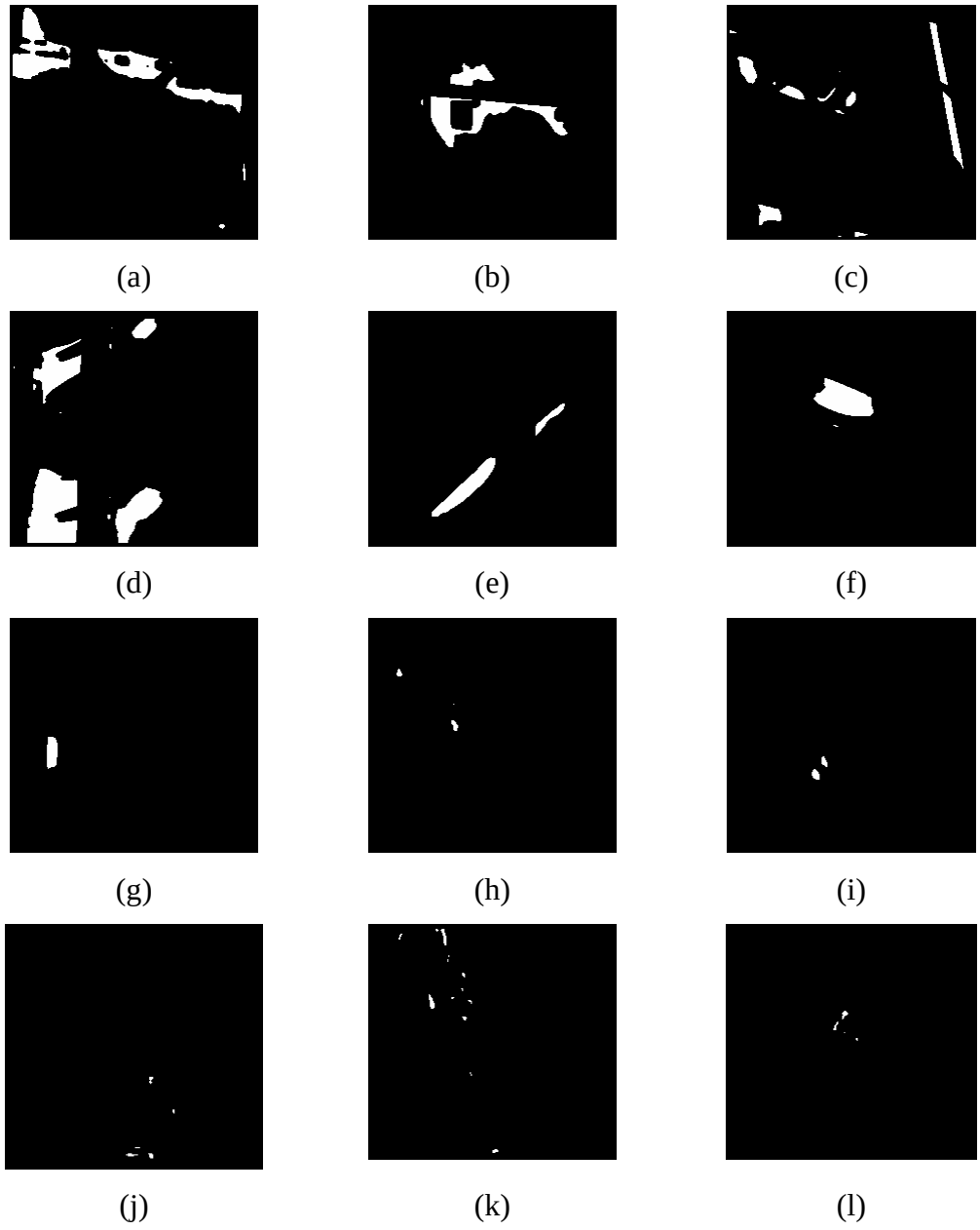

Figure 4.9 2nd level LIW image thresholded with MFT algorithm: (a) T = 172, (b) T = 106, (c) T = 176, (d) T = 193, (e) T = 83, (f) T = 111, (g) T = 28, (h) T = 36, (i) T = 63, (j) T = 52, (k) T = 111, (l) T = 76

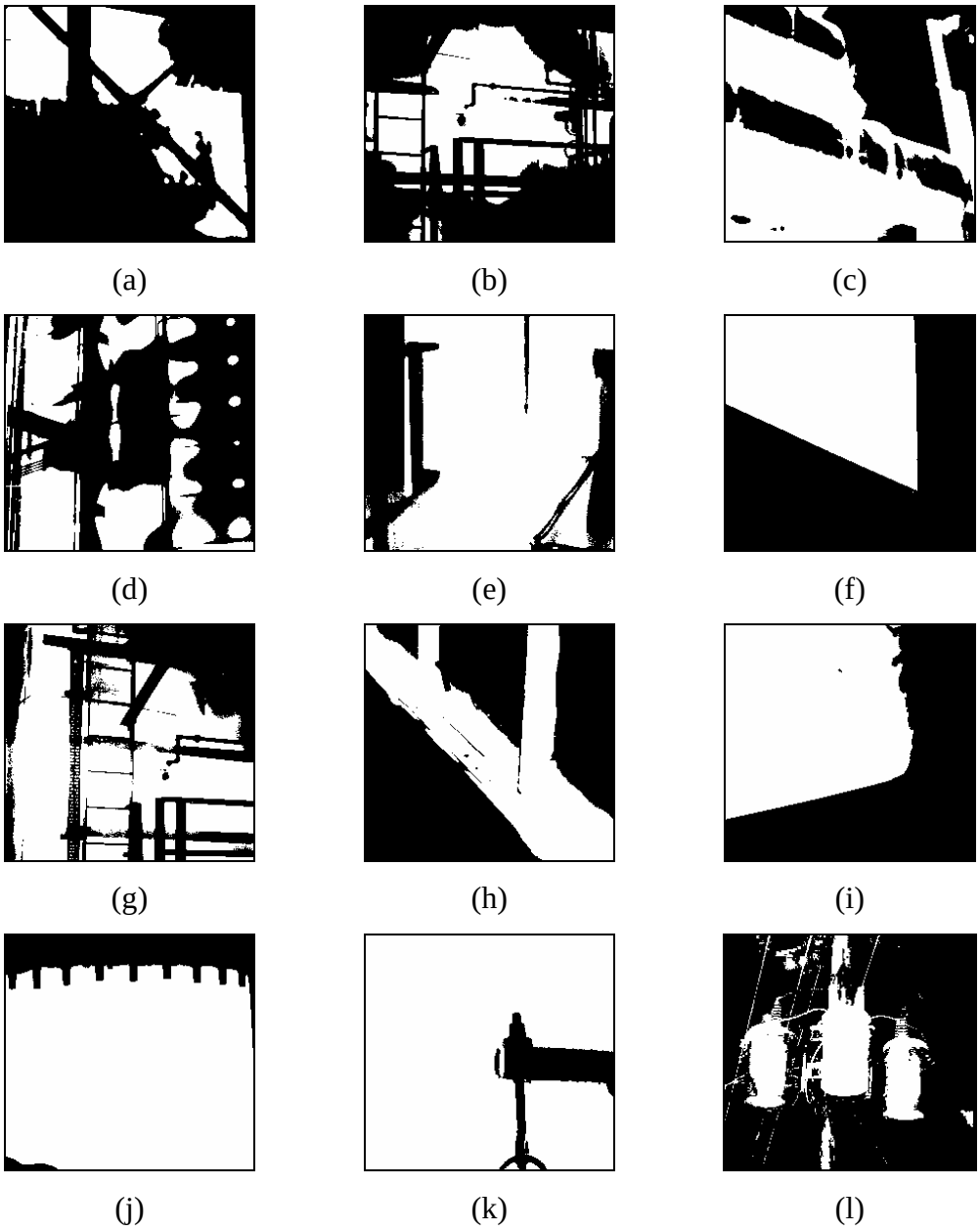

Figure 4.10 Defect detection using Otsu method: (a) T = 195, (b) T = 185, (c) T = 173, (d) T = 191, (e) T = 112, (f) T = 148, (g) T = 70, (h) T = 193, (i) T = 168, (j) T = 89, (k) T = 128, and (l) T = 101

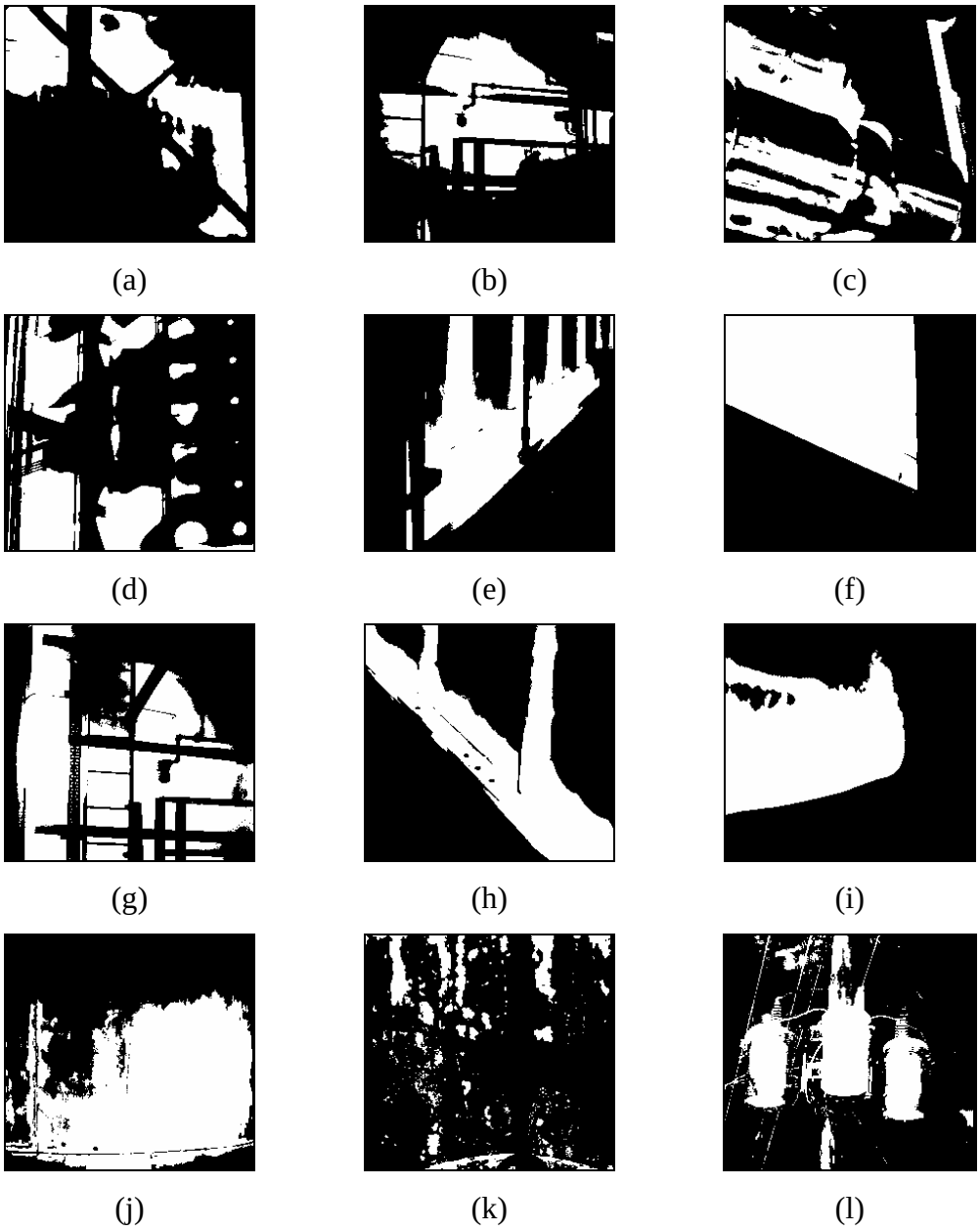

Figure 4.11 Defect detection using Hamadani method (with k_1 = 1 and k_2 = 2): (a) T = 204, (b) T = 196, (c) T = 200, (d) T = 202, (e) T = 158, (f) T = 160, (g) T = 103, (h) T = 206, (i) T = 191, (j) T = 169, (k) T = 228, and (l) T = 100

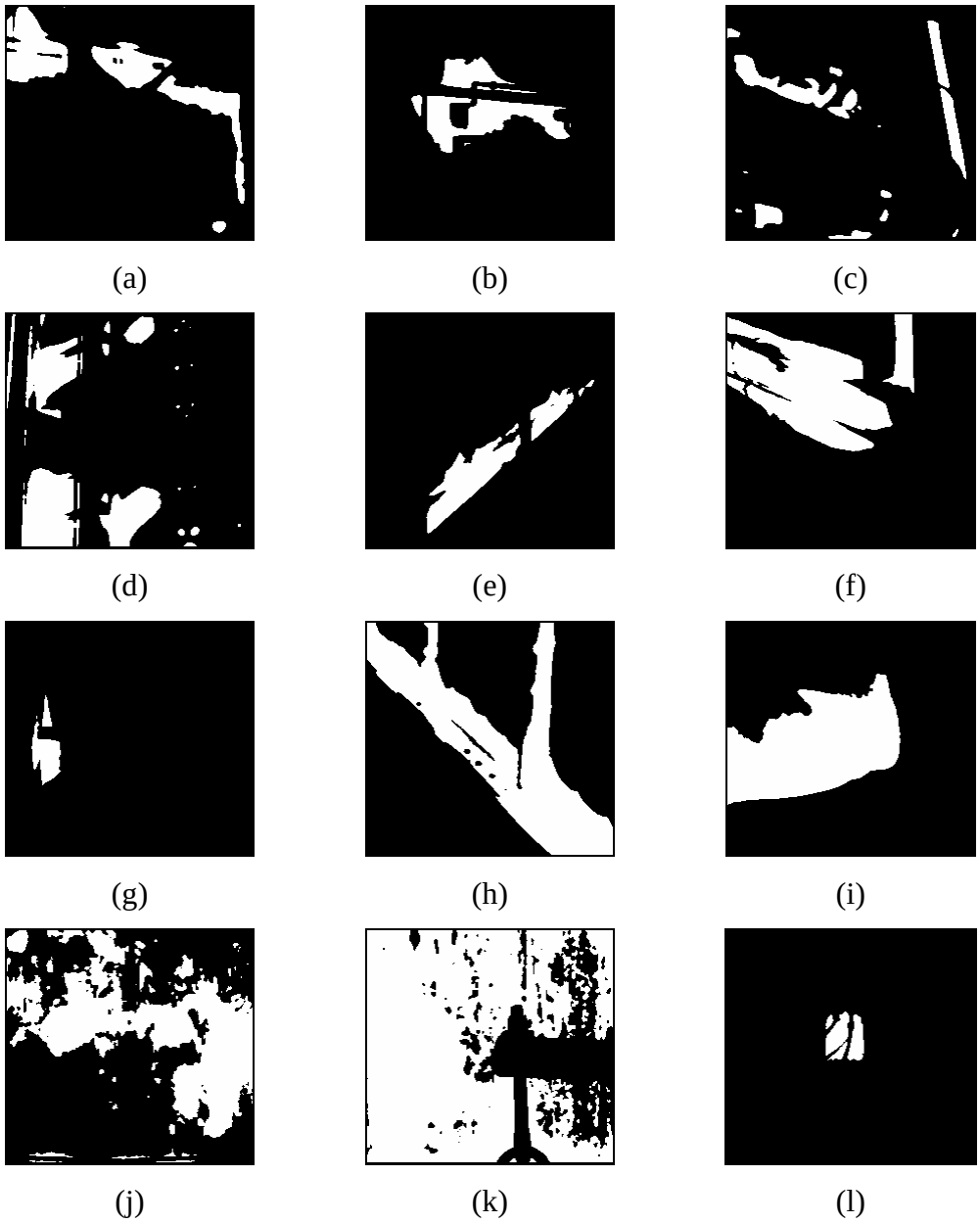

Figure 4.12 Defect detection using Otsu method on 1st level LIW image: (a) T = 119, (b) T = 114, (c) T = 118, (d) T = 124, (e) T = 93, (f) T = 77, (g) T = 77, (h) T = 48, (i) T = 46, (j) T = 81, (k) T = 76, and (l) T = 76

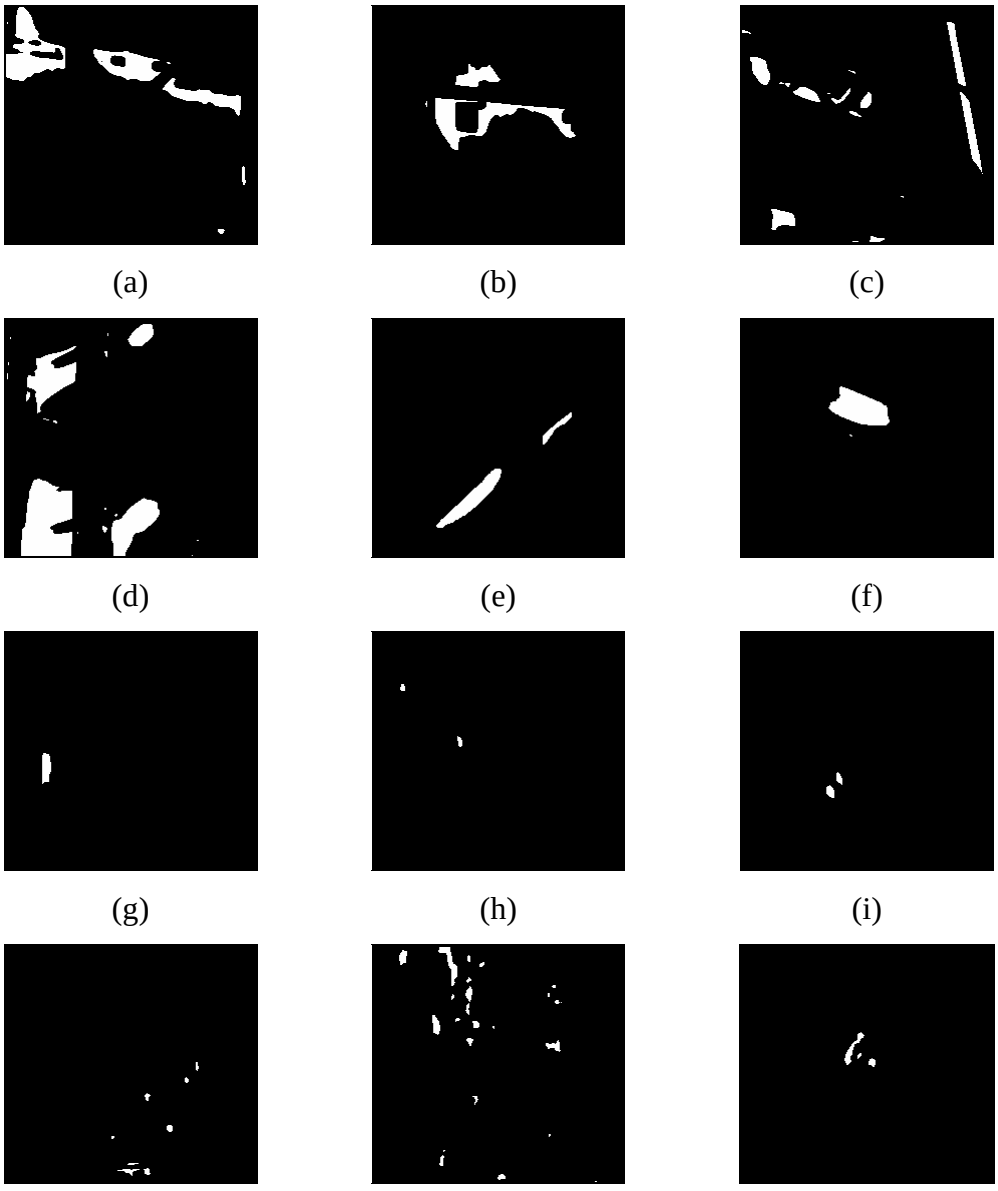

Figure 4.13 Defect detection using Otsu method on 2nd level LIW image: (a) T = 119, (b) T = 119, (c) T = 117, (d) T = 123, (e) T = 111, (f) T = 120, (g) T = 109, (h) T = 46, (i) T = 52, (j) T = 29, (k) T = 43, and (l) T = 33

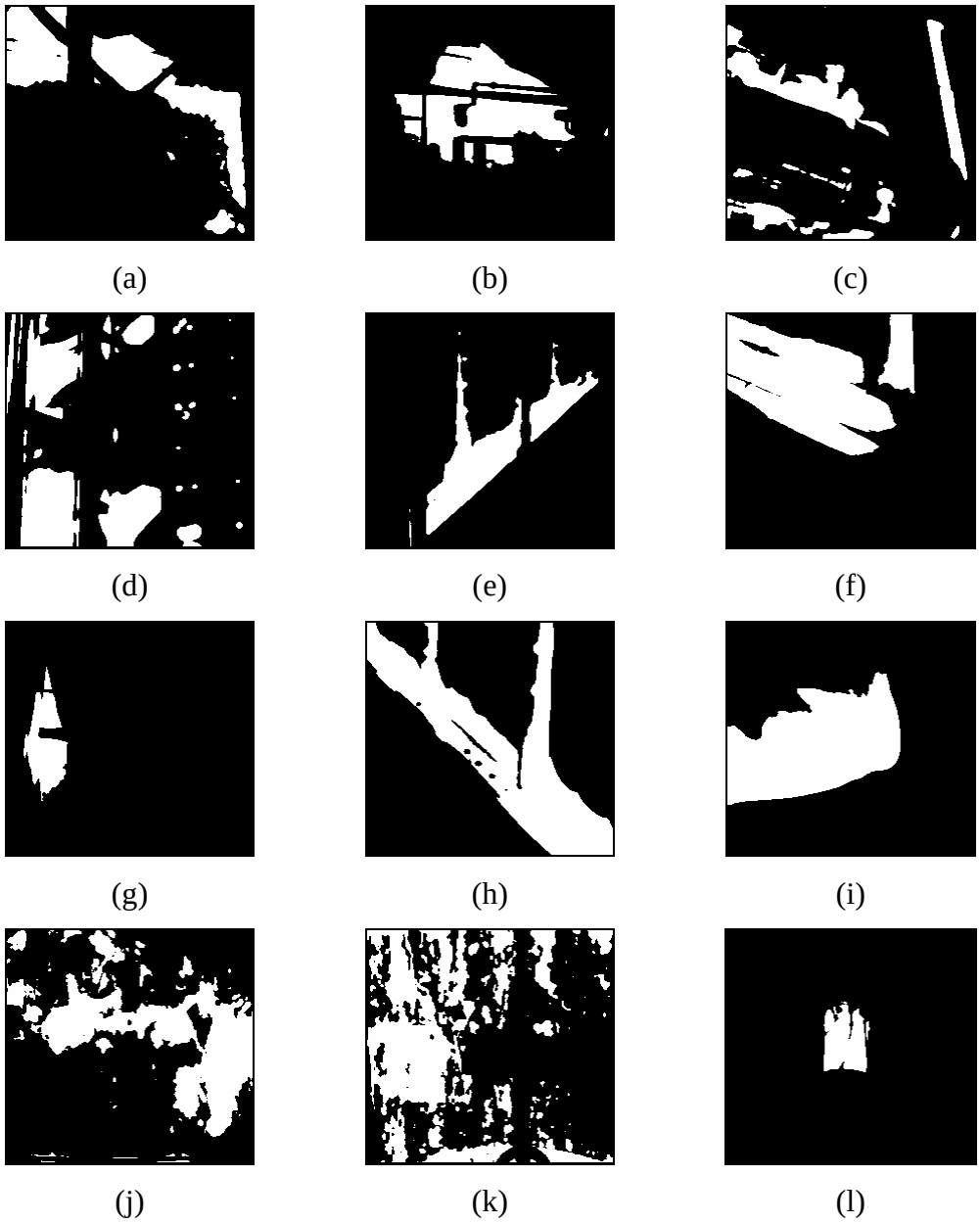

Figure 4.14 Defect detection using Hamadani method (with k_1 = 1 and k_2 = 2) on 1st level LIW image: (a) T = 57, (b) T = 46, (c) T = 46, (d) T = 67, (e) T = 30, (f) T = 56, (g) T = 11, (h) T = 51, (i) T = 44, (j) T = 90, (k) T = 117, (l) T = 10

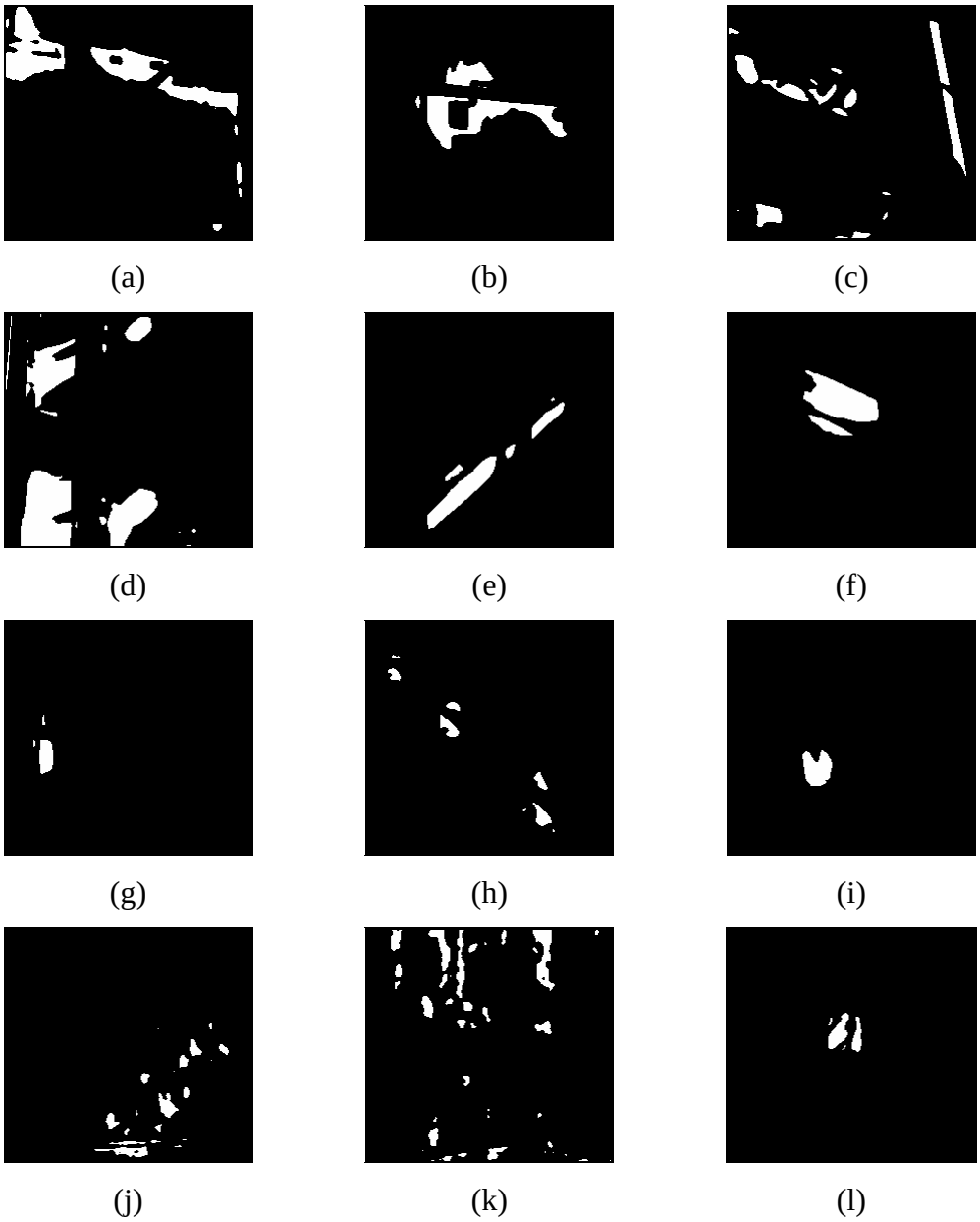

Figure 4.15 Defect detection using Hamadani method (with k_1 = 1 and k_2 = 2) on 2nd level LIW image: (a) T = 27, (b) T = 19, (c) T = 17, (d) T = 39, (e) T = 11, (f) T = 13, (g) T = 3, (h) T = 3, (i) T = 3, (j) T = 4, (k) T = 9, and (l) T = 3

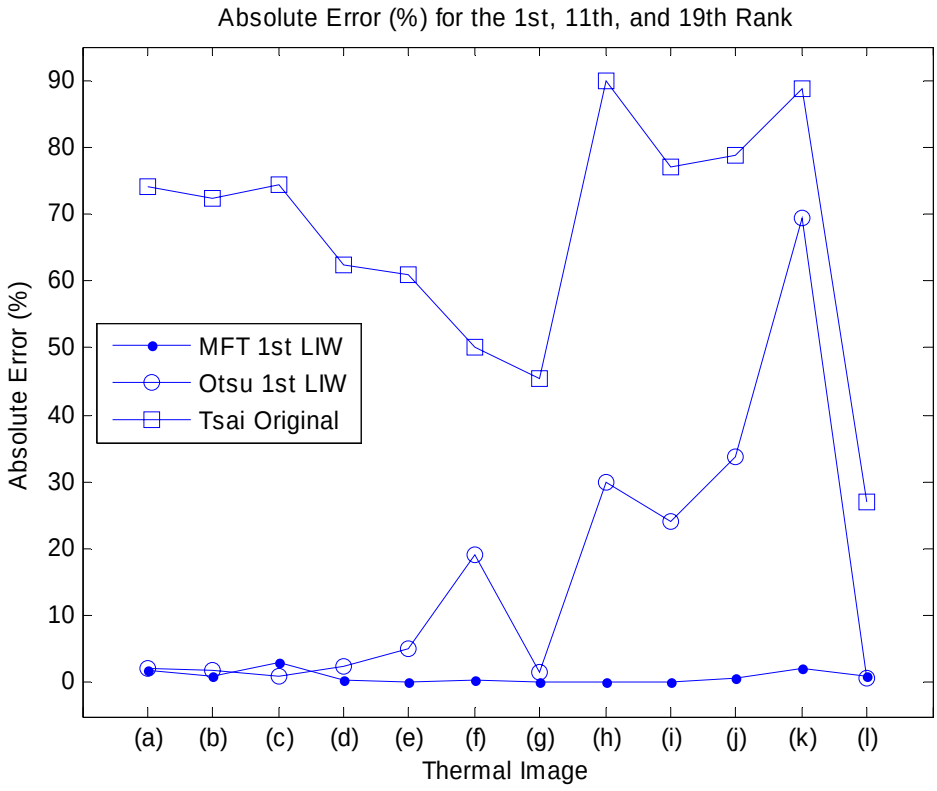

Figure 4.16 Absolute error ratio for the 1st, 11th, and 19th rank algorithm

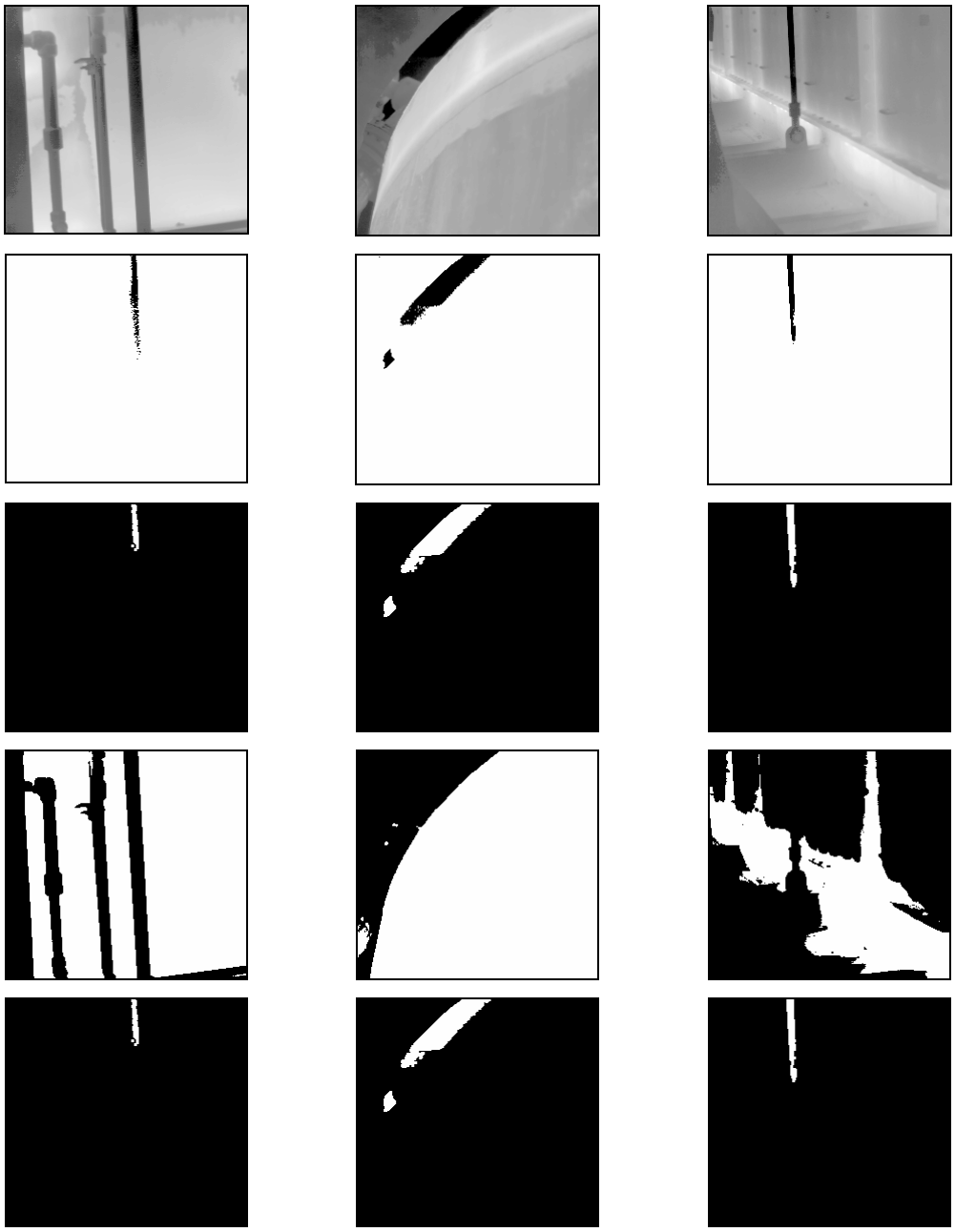

(a) (b) (c)

Figure 4.17 (from top to bottom) Thermal image dataset for *cold defect*, ground-truth, LIL image, thresholded by MFT algorithm on LIL image, thresholded by Otsu algorithm on original image, thresholded by Otsu algorithm on LIL image

CHAPTER 5

CONCLUSIONS AND SUGGESTIONS

5.1 Summary and Conclusions

In Chapter 1, the introduction on infrared thermography and its applications in petrochemical industry is described. Contributions are also highlighted. The scope and objective of the project are properly stated.

In Chapter 2, review on existing algorithms whether it is non-dedicated or dedicated algorithm for thermal image is presented. The advantages and disadvantages of these algorithms are addressed. A brief introduction of the proposed technique is given in the end of the chapter.

In Chapter 3, the proposed algorithm, *local intensities operation* (LIO), for pre-processing thermal image is discussed. Three simple thresholding algorithms (MAT, MRT, and MFT) for defect detection are introduced. Properties of these algorithms are discussed in the text.

In Chapter 4, experimental results showed the effectiveness of the proposed algorithms. Twelve thermal images were used for performance evaluation. Through benchmarking process, these algorithms are better compared to other existing algorithms. MFT thresholding algorithm when applied to a pre-processed thermal image with 1^{st} level LIW operation gives a satisfied result. Even, the pre-processed thermal image with LIW operation for any level when combined with non-dedicated defect detection algorithm will also give a very good result.

The proposed algorithms are simple and easy to implement yet give promising results. Therefore, the objective of this project for detecting defect in thermal image has been achieved.

5.2 Limitations

Looking at the contributions made in this work, it is possible to automatically detect defects as depicted in thermal images. This automatic interpretation will eliminate the error prone to arise if it is done by human operator. It can then increase the efficiency and contribute to the productivity of the whole chains in a petrochemical site.

However, this method assumes that the thermal image is noise or thermal masses free, hence any existence of noise or thermal masses in an image will also be considered as a defective pattern, which can then affect the performance on defect detection result.

Local intensities operation (LIW and LIL) tends to shrink the shape of the defect. Since this project does not concern on the shape, so this issue is not a problem. But, if one thinks that the shape is important, for instance for defect sizing, further processing need to be incorporated before an accurate decision can be obtained.

5.3 Suggestions for Future Research

Based on the related problems discussed in the previous section, some of the future work can be suggested as follows:

- By existence of noise and thermal masses depicted in thermal image, the proposed algorithms need to be further enhanced.

- If shape of the defects is important, a further algorithm needs to be developed to preserve this shape. This report proposes employing morphological dilation operation, but another technique that may suitable may also be investigated.

- Performance of the proposed algorithms on color thermogram has not been investigated. This study could open a new research area in infrared thermography image processing application.

REFERENCES

Abutaleb, A. S. (1989). Automatic Thresholding of Gray-level Pictures using Two-Dimensional Entropy. *Computer Vision, Graphics, and Image Processing.* 47: 22-32.

Araki, S., Nomura, H., and Wakami, N. (1993). Segmentation of Thermal Images using the Fuzzy C-Means Algorithm. *Proceedings of IEEE.* 719-724.

Baraldi, A. and Parmiggiani, F. (1995). An Investigation of the Textural Characteristics Associated with Gray Level Cooccurrence Matrix Statistical Parameters. *IEEE Transactions on Geoscience and Remote Sensing.* 33(2): 293-304.

Bezdek, J. C. (1981). *Pattern Recognition with Fuzzy Objective Function Algorithms.* New York: Plenum Press.

Bonabeau, E., Dorigo, M., and Theraulez, G. (1999). *Swarm Intelligence: from Natural to Artificial Systems.* New York: Oxford University Press.

Bonin, R. G. (2003). IR Applications for Process Vessels. *Proceedings of InfraMation 2003.* Las Vegas, Nevada. Oct. 13-16, 2003.

Chanda, B. and Majumder, D. D. (2000). *Digital Image Processing and Analysis*. New Delhi: Prentice-Hall of India Private Limited.

Chang, J. S., Liao, H. Y. M., Hor, M. K., Hsieh, J. W., and Chern, M. Y. (1997). New Automatic Multi-level Thresholding Technique for Segmentation of Thermal Images. *Image and Vision Computing.* 15: 23-34.

Cho, S., Haralick, R., and Yi, S. (1989). Improvement of Kittler and Illingworth's Minimum Error Thresholding. *Pattern Recognition.* 22: 609-617.

D'Orazio, T., Guaragnella, C., Leo, M., and Spagnolo, P. (2005). Defect Detection in Aircraft Composites by using a Neural Approach in the Analysis of Thermographic Images. *NDT&E International.* 38: 665-673.

Darabi, A. (2000). Detection and Estimation of Defect Depth in Infrared Thermography using Artificial Neural Networks and Fuzzy Logic. Université Laval, Canada: Ph.D Thesis.

Darabi, A. and Maldague, X. (2002). Neural Network based Defect Detection and Depth Estimation in TNDE. *NDT&E International.* 35: 165-175.

Du, Y., Chang, C.-I., and Thouin, P. D. (2004). Unsupervised Approach to Color Video Thresholding. *Optical Engineering.* 43(2): 282-289.

Dufour, M. B. (2005). Quantification of Air Leaks through the Building Envelope using Infrared Thermography. Concordia University, Canada: M.Ap.Sc Thesis.

Feng, D., Wenkang, S., Liangzhou, C., Yong, D., and Zhenfu, Z. (2005). Infrared Image Segmentation with 2-D Maximum Entropy Method based on Particle Swarm Optimization (PSO). *Pattern Recognition Letters.* 26: 597-603.

Gardner, W. E. (1992). *Improving the Effectivenes and Reliability of Non-destructive Testing.* Oxford, England: Pergamon Press, Ltd.

Gaussorgues, G. (1994). *Infrared Thermography*. Cambridge: Chapman & Hall.

Giardina, C. R. and Dougherty, E. R. (1988). *Morphological Methods in Image and Signal Processing.* Prentice-Hall, Inc.

Glasbey, C. A. (1993). An Analysis of Histogram-based Thresholding Algorithms. *CVGIP: Graphical Models and Image Processing.* 55(6): 532-537.

Gonzalez, R. C. and Woods, R. E. (2002). *Digital Image Processing*. (2nd ed.). Upper Saddle River, New Jersey: Prentice-Hall, Inc.

Gonzalez, R. C., Woods, R. E., and Eddins, S. L. (2004). *Digital Image Processing using MATLAB*. Upper Saddle River, New Jersey: Prentice-Hall, Inc.

Griswold, J. (1946). *Fuels, Combustion, and Furnaces.* McGraw-Hill Book Company, Inc.

Haddon, J. F. and Boyce, J. F. (1990). Unification of Image Segmentation and Edge Detection. *IEE Proceedings.* 137, Pt. I(3): 129-135.

Haddon, J. F. and Boyce, J. F. (1993). Co-occurrence Matrices for Image Analysis. *Electronics & Communication Engineering Journal.* 71-83.

Hamadani, N. (1981). *Automatic Target Cueing in IR Imagery*. WPAFB, Ohio: Master's Thesis.

Haralick, R. M. (1979). Statistical and Structural Approaches to Texture. *Proceedings of the IEEE.* 67(5): 786-808.

Haralick, R. M., Shanmugam, K., and Dinstein, I. (1973). Textural Features for Image Classification. *IEEE Transactions on Systems, Man, and Cybernetics.* SMC-3(6): 610-621.

Jin, W., Ya, Q., Jian, L., and Jinwen, T. (2004). Infrared Image Segmentation via Intelligent Genetic Algorithm based on Maximum Entropy. *Proceedings of ICSP '04.* 789-792.

Kaplan, H. (1993). *Practical Applications of Infrared Thermal Sensing and Imaging Equipment.* Bellingham, Washington: SPIE-The International Society for Optical Engineering.

Kapur, J. N., Sahoo, P. K., and Wong, A. K. C. (1985). A New Method of Gray Level Picture Thresholding using the Entropy of the Histogram. *Computer Vision, Graphics, and Image Processing.* 29: 273-285.

Khotanzad, A. and Bouarfa, A. Image Segmentation by a Parallel, Non-parametric Histogram based Clustering Algorithm. *Pattern Recognition.* 23(9): 961-973.

Kittler, J. and Illingworth, J. (1985). On Threshold Selection using Clustering Criteria. *IEEE Transactions on Systems, Man, and Cybernetics.* 15(5): 652-655.

Kittler, J. and Illingworth, J. (1986). Minimum Error Thresholding. *Pattern Recognition.* 19: 41-47.

Le, S. U., Chung, S. Y., and Park, R. H. (1990). A Comparative Performance Study of Several Global Thresholding Techniques for Segmentation. *Graphical Model and Image Processing.* 52: 171-190.

LeClercq, A. J. (2003). The Art of Furnace Tube Skin Temperatur Analysis. *Proceedings of InfraMation 2003.*

Levine, M. D. (1985). *Vision in Man and Machine*. New York: McGraw-Hill, Inc.

Levitt, J. (2003). *Complete Guide to Preventive and Predictive Maintenance.* New York: Industrial Press, Inc.

Liao, P. S., Chen, T. S., and Chung, P. C. (2001). A Fast Algorithm for Multilevel Thresholding. *Journal of Information Science and Engineering.* 17: 713-727.

Lin, K. C. (2002). Fast Image Thresholding by Finding the Zero(s) of the First Derivative of Between-class Variance. *Machine Vision and Applications.* 13: 254-262.

Lo, T. Y. and Choi, K. T. W. (2004). Building Defects Diagnosis by Infrared Thermography. *Structural Survey.* 22(5): 259-263.

Maldague, X. P. V. (1993). *Nondestructive Evaluation of Materials by Infrared Thermography*. Springer-Verlag London Limited.

Maldague, X. P. V. (2001). *Theory and Practice of Infrared Technology for Nondestructive Testing.* John Wiley & Sons, Inc.

Maldague, X., Krapez, J. C., and Poussart, D. (1990). Thermographic Nondestructive Evaluation (NDE): An Algorithm for Automatic Defect Extraction in Infrared Images. *IEEE Transactions on Systems, Man, and Cybernetics.* 20(3): 722-725.

May, K. B. (2003). Predictive Maintenance Inspections – Boilers in Fossil Power Plants. *Proceedings of InfraMation 2003.*

Minor, L. G. and Sklansky, J. (1981). Detection and Segmentation of Blobs in Infrared Images. *IEEE Transactions on Systems, Man, and Cybernetics.* SMC-11(3): 194-201.

Mobley, R. K. (1990). *An Introduction to Predictive Maintenance*. New York: Van Nostrand Reinhold.

Nakagawa, Y. and Rosenfeld, A. (1978). Some Experiments on Variable Thresholding. *Pattern Recognition.* 11: 191-204.

Ng, H. F. (2006). Automatic Thresholding for Defect Detection. *Pattern Recognition Letters.* 27: 1644-1649.

Nyholt, J. J. (2000). Infrared Thermography in BP Amoco – Petrochemical Applications. *Proceedings of InfraMation 2000.*

Ohliger, A. A. (2002). Using Infrared Thermography on Offshore Platform Equipment. *Proceedings of InfraMation 2004.*

Ohliger, A. A. (2003). Horsehead (beam) pump Infrared Analysis. *Proceedings of InfraMation 2003.*

Ohliger, A. A. O. and Alvarado, G. E. (2001). Texaco's Use of Infrared on Fired Process Heaters. *Proceedings of InfraMation 2001.*

Olivo, J. C. (1994). Automatic Threshold Selection using the Wavelet Transform. *CVGIP: Graphical Models and Image Processing.* 56: 205-218.

Omar, M. A. (2005). *Dedicated Processing Routines for Thermography Facial and Pulsed Subsurface Non-destructive Testing Industrial Applications.* University of Kentucky, Lexington: PhD Thesis.

Omar, M., Hassan, M. I., Saito, K., and Allo, R. (2005). IR Self-referencing Thermography for Detection of In-depth Defects. *Infrared Physics & Technology*. 46: 283-289.

Otsu, N. (1979). A Threshold Selection Method from Gray-level Histograms. *IEEE Transactions on Systems, Man, and Cybernetics*. SMC-9(1): 62-66.

Parker, J. R. (1997). *Algorithms for Image Processing and Computer Vision*. USA: John Wiley & Sons, Inc.

Parsi, B. K. and Parsi, B. K. (2001). Improved Image Thresholding for Object Extraction in IR Images. *Proceedings of 2001 International Conference on Image Processing.* Thessaloniki, Greece: Oct. 7-10, 2001. 1: 758-761.

Pitas, I. (1993). *Digital Image Processing Algorithms*. Cambridge: Prentice Hall International (UK) Ltd.

Qi, H., Kuruganti, P. T., and Liu, Z. (2002). Early Detection of Breast Cancer using Thermal Texture Maps. *Proceedings of IEEE.* 309-312.

Ridler, T. and Calvard, S. (1979). Picture Thresholding using Iterative Selection Method. *IEEE Trans. Syst., Man, and Cybernet.* SMC-9: 311.

Ritter, G. X. and Wilson, J. N. (2001). *Handbook of Computer Vision Algorithms in Image Algebra*. (2nd ed.). Boca Raton, Florida: CRC Press LLC.

Rosenfeld, A. and De la Torre, P. (1983). Histogram Concavity Analysis as an Aid in Threshold Selection. *IEEE Trans. Syst. Man Cybern.* SMC-13: 231-235.

Sahoo, P. K., Soltani, S., Wong, A. K.C., and Chen, Y. C. (1988). A Survey of Thresholding Techniques. *Computer Vision, Graphics, and Image Processing.* 41: 233-260.

Šapina, R. (2001). Computing Textural Features based on Co-occurrence Matrix for Infrared Images. *Proceedings of the 2nd International Symposium on Image and Signal Processing and Analysis.* 373-376.

Sezgin, M. and Sankur, B. (2001). Selection of Thresholding Methods for Non-destructive Testing Applications. *Proceedings of the 2001 IEEE International Conference on Image Processing (ICIP 2001).* 13(1): 145-165.

Sezgin, M. and Sankur, B. (2003). Image Multi-thresholding based on Sample Moment Function. *Proceedings of the 2003 IEEE International Conference on Image Processing (ICIP 2003).* 13(1): 145-165.

Sezgin, M. and Sankur, B. (2004). Survey over Image Thresholding Techniques and Quantitative Performance Evaluation. *Journal of Electronic Imaging*. 13(1): 145-165.

Silverman, J., Rotman, S. R., and Caefer, C. E. (2004). Segmentation of Multi-dimensional Infrared Imagery from Histograms. *Infrared Physics & Technology*. 45: 191-200.

Sims, D. L. (2001). Using Infrared Imaging on Production Tanks & Vessels. *Proceedings of InfraMation 2001*.

Tao, W., Jin, H., and Liu, L. (2007). Object Segmentation using Ant Colony Optimization Algorithm and Fuzzy Entropy. *Pattern Recognition Letters.* 28: 788-796.

Trier, O. D. and Jain, A. K. (1995). Goal-Directed Evaluation of Binarization Methods. *IEEE Transactions on Pattern Analysis and Machine Intelligence*. 17(12): 1191-1201.

Tsai, W. H. (1985). Moment-Preserving Thresholding: A New Approach. *Computer Vision, Graphics, and Image Processing.* 29: 377-393.

Wang, W., Zeng, Y., Ma, D., Jin, Z., Wu, H., Yuan, C., and Yuan, Y. (2004). Clinical Study on using Thermal Texture Maps in SARS diagnosis. *Proceedings of the 26th Annual International Conference of the IEEE EMBS*. 5258-5264.

Weigle, R. K. (2005). Applications of Infrared Thermography for Petrochemical Process Heaters. *Proceedings of the SPIE Thermosense XXVII*. 5782: 100-108.

Weszka, J. S. and Rosenfeld, A. (1978). Threshold Evaluation Techniques. *IEEE Transactions on Systems, Man, and Cybernetics*. SMC-8: 627-629.

Whitcher, A. (2003). Thermographic Monitoring of Refractory Lined Petroleum Refinery Equipment. *Proceedings of InfraMation 2004.*

Willis, J. (2004). Lagged Pipe Survey. *Proceedings of InfraMation 2004.*

Wu, J., Li, J., Liu, J., and Tian, J. (2004). Infrared Image Segmentation via Fast Fuzzy C-Means with Spatial Information. *Proceedings of the 2004 IEEE International Conference on Robotics and Biomimetics.* Aug. 22-26, 2004. Shenyang, China. 742-745.

Wu, S. and Amin, A. (2003). Automatic Thresholding of Gray-level using Multi-stage Approach. *Proceedings of the Seventh International Conference on Document Analysis and Recognition (ICDAR 2003).*

Yasnoff, W. A., Mui, J. K., and Bacus, J. W. (1977). Error Measures for Scene Segmentation. *Pattern Recognition.* 9: 217-231.

APPENDIX A

INFRAMETRICS PM 390 SPECIFICATION

Manufacturer	Inframetrics, Inc.
Model	PM 390
Measurement range	-20^{o} to $+450^{o}$ (extended to $+1500^{o}$C with filter)
Sensitivity	< 0.1^{o}C at 30^{o}C
Accuracy	±2% or ±2 ^{o}C
Display type	Viewfinder Color LCD eyepiece
Video output	RS 170, NTSC, S-VIDEO, CCIR, PAL
Infrared detector	PiSi/CMOS 256×256 FPA with variable integration
Spectral band	3.4 to 5 micron
IR dynamic range	16 bits
Operating temperature	-15^{o}C to +50 ^{o}C, IEC 359
Storage temperature	-40^{o}C to +70 ^{o}C, IEC 359
Shock/vibration	70g, IEC 68-2-6
Focus range	9″ to infinity